# Validation of operational ozone profiles from the Ozone Monitoring Instrument

M. Kroon,[1] J. F. de Haan,[1] J. P. Veefkind,[1] L. Froidevaux,[2] R. Wang,[3] R. Kivi,[4] and J. J. Hakkarainen[5]

Received 22 September 2010; revised 18 May 2011; accepted 28 June 2011; published 20 September 2011.

[1] In this paper we present the validation results of the operational vertical ozone profiles retrieved from the nadir observations by the Ozone Monitoring Instrument (OMI) aboard the NASA Earth Observing System (EOS) Aura platform. The operational ozone profile retrieval algorithm was developed at the Royal Netherlands Meteorological Institute and the OMI mission data has been processed and made publicly available. Advantages of these nadir sounded ozone profiles are the excellent spatial resolution at nadir and daily global coverage while the vertical resolution is limited to 6–7 km. Comparisons with well-validated ozone profile recordings by the Microwave Limb Sounder (MLS) and the Tropospheric Emission Spectrometer (TES), both aboard the NASA EOS-Aura platform, provide an excellent opportunity for validation because of the large amount of collocations with OMI due to the instruments significant geographical overlap. In addition, comparisons with collocated ozone profiles from the Stratospheric Aerosol and Gas Experiment (SAGE-II), the Halogen Occultation Experiment (HALOE), the Global Ozone Monitoring by the Occultation of Stars (GOMOS) and the Optical Spectrograph and Infrared Imager System (OSIRIS) satellite instruments and balloon-borne electrochemical concentration cell (ECC) ozonesondes are presented. OMI stratospheric ozone profiles are found to agree within 20% with global correlative data except for both the polar regions during local spring. For ozone in the troposphere OMI shows a systematic positive bias versus the correlative data sets of order 60% in the tropics and 30% at midlatitude regions. The largest source of error in the tropospheric ozone profile is the fit to spectral stray light in the operational algorithm.

**Citation:** Kroon, M., J. F. de Haan, J. P. Veefkind, L. Froidevaux, R. Wang, R. Kivi, and J. J. Hakkarainen (2011), Validation of operational ozone profiles from the Ozone Monitoring Instrument, *J. Geophys. Res.*, *116*, D18305, doi:10.1029/2010JD015100.

## 1. Introduction

[2] A thorough understanding of the Earth's ozone layer, particularly in the upper troposphere to lower stratosphere exchange regions in the tropics and during the southern hemisphere ozone hole season over Antarctica, requires three-dimensional global monitoring with a good spatial and temporal resolution. Current endeavors by space-borne sounders to obtain such information include the Microwave Limb Sounder (MLS) and Tropospheric Emission Spectrometer (TES) instruments aboard the NASA EOS-Aura platform, the Global Ozone Monitoring by the Occultation of Stars (GOMOS) instrument aboard the ESA ENVISAT platform and the Optical Spectrograph and Infrared Imager System (OSIRIS) aboard the Swedish Odin satellite. Here we present the validation of vertical ozone profiles operationally retrieved from the UVVIS nadir observations by the Ozone Monitoring Instrument (OMI) using an algorithm developed at the Royal Netherlands Meteorological Institute (KNMI) that is based on the optimal estimation retrieval technique. The OMI vertical ozone profiles provide maps of the global ozone layer in three dimensions on a daily basis with a horizontal resolution of at least 65 km x 48 km and capturing the vertical ozone structures from the surface up to 65 km in 18 pressure layers, with a vertical resolution of at least 6 km. These retrievals constitute a comprehensive data set to study the spatiotemporal distribution of ozone everywhere on the globe. This data set can potentially yield accurate estimates of tropospheric ozone columns either by sampling the retrieved profiles themselves or by subtracting a stratospheric column estimate obtained from the ozone profiles from a total ozone column estimate obtained at similar or longer wavelengths by means of the well-validated OMI-TOMS or OMI-DOAS

[1] Department of Climate and Seismology, Royal Netherlands Meteorological Institute, De Bilt, Netherlands.
[2] Jet Propulsion Laboratory, California Institute of Technology, Pasadena, California, USA.
[3] School of Earth and Atmospheric Sciences, Georgia Institute of Technology, Atlanta, Georgia, USA.
[4] Arctic Research Centre, Finnish Meteorological Institute, Sodankylä, Finland.
[5] Department of Earth Observation, Finnish Meteorological Institute, Helsinki, Finland.


0148-0227/11/2010JD015100

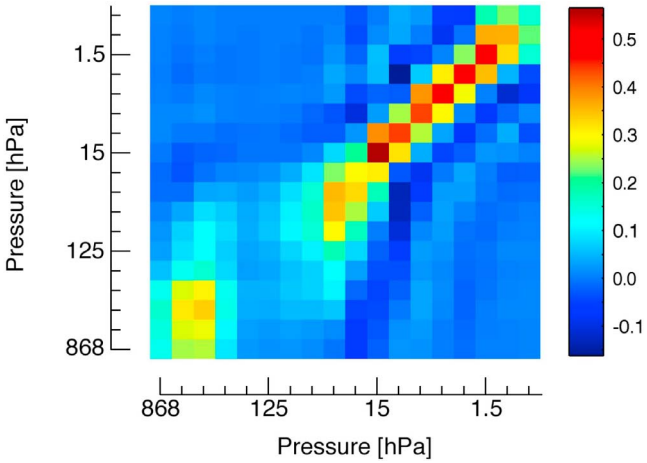


**Figure 1.** Graphical display of the averaging kernel of the OMI operational ozone profile retrieval indicating where the information present in the OMI vertical ozone profile (horizontal axis) originates from in the atmosphere (vertical axis). The plot reveals that ozone structures in the stratosphere (lowest pressures) are captured well whereas in the troposphere one cannot distinguish between one level and another.

ozone column techniques [*Kroon et al.*, 2008]. In this paper we quantify the quality of the OMI operational ozone profiles by performing a comparison against the well validated profiles provided by the MLS, TES, SAGE-II, HALOE, GOMOS and OSIRIS satellite instruments and against balloon-borne electrochemical concentration cell (ECC) ozonesondes.

## 2. OMI Aboard EOS-Aura

[3] The NASA Earth Observing System (EOS) Aura satellite was launched on the 15th of July 2004 into a sun-synchronous polar orbit at about 705 km altitude with a 98.2° inclination and ascending node equator-crossing time at roughly 13:45 LT [*Schoeberl et al.*, 2006]. The Dutch-Finnish Ozone Monitoring Instrument (OMI) aboard the NASA EOS-Aura satellite is a compact nadir viewing, wide swath, ultraviolet-visible (270–500 nm) push-broom imaging spectrometer that provides daily global coverage with high spatial and spectral resolution without scanning mirrors in the spatial or spectral dimensions [*Levelt et al.*, 2006a, 2006b]. OMI measures backscattered solar radiance in the dayside portion of each orbit and solar irradiance near the northern hemisphere terminator once per day in three channels covering the 270–500 nm wavelength range (UV-1: 270–310 nm, UV-2: 310–365 nm, visible: 350–500 nm) at spectral resolutions of 0.42–0.63 nm. The OMI data products are derived from the ratio of Earth radiance and solar irradiance and come in the form of Level-2 orbit files that contain trace gas abundances (e.g., O3, NO2, SO2, HCHO, BrO, CHOCHO, OClO) as well as UV-absorbing aerosol and cloud properties. All OMI data are publicly available at the NASA DISC systems (please visit http://disc.sci.gsfc.nasa.gov/Aura/data-holdings/OMI/index.shtml). The time period covered by this analysis is the OMI mission data available at the time of writing, from October 2004 to December 2010.

## 3. Short History of the Ozone Profile Retrieval

[4] Already for decades scientists have worked on obtaining accurate ozone vertical profiles from satellite observations of UV backscattered solar radiation. The measurements by the Solar Backscatter Ultraviolet Radiometer (SBUV) instrument series, the first launched in 1984, were used to chart the distribution of stratospheric ozone with altitude by *Bhartia et al.* [1996]. The Global Ozone Monitoring Experiment (GOME) instrument was launched in 1995 and ozone profile retrievals from GOME data were subsequently performed by *Chance et al.* [1997], *Munro et al.* [1998], *Hoogen et al.* [1999], *Hasekamp and Landgraf* [2001], *van der A et al.* [2002], *Müller et al.* [2003], and *Liu et al.* [2005]. A brief review of the methods employed is given by *Liu et al.* [2005]. Except for the work by *Hasekamp and Landgraf* [2001] and *Müller et al.* [2003], the Optimal Estimation methodology developed by *Rodgers* [2000] was used as the retrieval method in these papers. Optimal estimation provides a full characterization of a profile retrieval, which allows for robust comparison between the estimated profile and other data sets. Convergence diagnostics were discussed by *Mijling et al.* [2010] which led to an improved quality of the data set mainly by mitigating effects of instrumental errors and incorrect a-priori data. Ozone profiles derived from GOME-2 measurements during Antarctic ozone hole conditions have been discussed by *van Peet et al.* [2009] which showed that accurate ozone profiles can be retrieved for these extreme conditions. Finally, *Liu et al.* [2010a] discussed their ozone profile retrievals from OMI measurements. The operational OMI ozone profile data product used in this study [*van Oss et al.*, 2001] is labeled OMO3PR and its retrieval algorithm is described below.

## 4. Brief Description of the Operational OMI Ozone Profile Algorithm

[5] The operational ozone profile algorithm is based on the physical mechanism of a 4 orders of magnitude decrease in the ozone absorption cross section from 330 nm to 270 nm. Envisage that light with a wavelength of 270 nm penetrates the atmosphere to an altitude of roughly 60 km while much of the incident light at 330 nm reaches the ground surface. Hence, a change in ozone in the troposphere affects the radiance spectrum at longer wavelengths while a change in ozone at the top of the atmosphere affects the radiance at all wavelengths. The retrieval algorithm is based on optimal estimation [*Rodgers*, 2000] where the amount of ozone in each atmospheric layer is adjusted such that the difference between the modeled and measured sun-normalized radiance is minimal. This approach is common practice nowadays for the retrieval of nadir ozone profiles from UVVIS spectra recorded by a number of satellite based platforms such as OMI, SCIAMACHY and GOME-2, differing mainly in the auxiliary information such as surface albedo and a-priori climatologies, and in forward model components. The measurements are taken from the OMI UV1 channel (270.0–308.5 nm) and the first part of the OMI UV2 channel (311.5–330.0 nm). The spectra of two adjacent across track

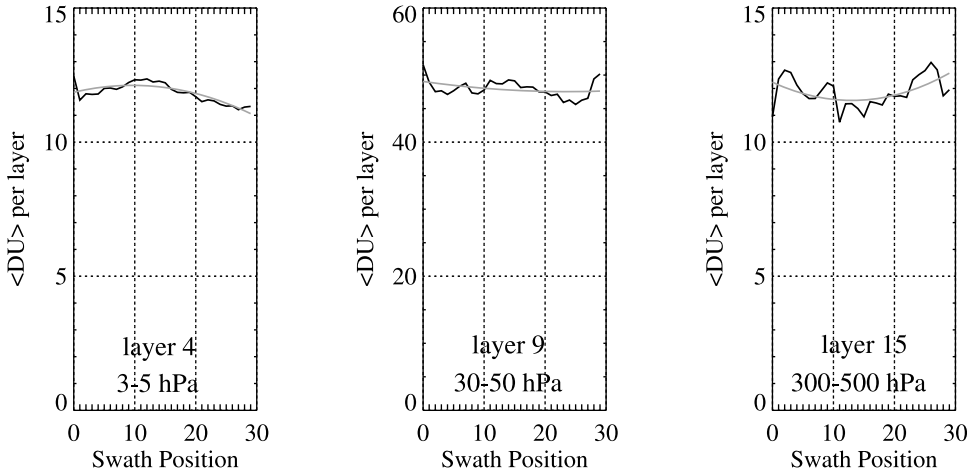


**Figure 2.** Cross track average for the month of October 2004 (2004–10) for the orbit phase range 153°–162° plotted for selected pressure layers (see insets). Black line shows the average data and gray line shows a second order polynomial fit to the data.

ground pixels in the UV2 channel are combined to obtain the spectrum of the same ground pixel in the UV1 channel. Hence, the ozone profile data product contains 30 across track ground pixels rather than the usual 60 for the other operational level-2 data products. Small differences in optical alignment between both detector channels are dealt with by assuming that the surface albedo or cloud albedo for the two channels can be different. The algorithm uses the newly developed LABOS radiative transfer model, which replaces the 4/6 stream Lidort-A model [*van Oss and Spurr*, 2002] that is currently used for GOME and GOME-2. LABOS includes an approximate treatment of rotational Raman scattering, pseudo spherical correction for direct sunlight, and corrections for the initial assumption that the atmospheric layers are homogeneous. OMI is equipped with a polarization scrambler. Therefore the RTM calculations should provide the radiance. However, polarization needs to be taken into account to get proper radiances when multiple scattering is involved. Instead of using polarized radiative transfer code we use a scalar version for the RTM calculations and account for polarization effects on the radiance by using a look-up table that is calculated with an adding doubling code [*de Haan et al.*, 1987]. The main reason for doing this is to improve the efficiency of the RTM calculations by about a factor of 4. Ozone cross sections are from *Malicet et al.* [1995]. A quadratic polynomial in the temperature is used for each wavelength and the coefficients of the polynomial are obtained from fitting data measured at 218, 228, 243, and 295 K. Global ECMWF pressure and temperature profiles are used in the retrieval. Forward calculations are performed in the wavelength range 267–332 nm on a sufficiently fine wavelength grid such that after interpolation the error in the reflectance is less than about 0.2% for any wavelength considered. In this interpolation our knowledge of the wavelength dependence of the absorption cross section of ozone is used. This procedure facilitates convolutions with the rotational Raman line spectrum and convolutions with the OMI slit function [*Dirksen et al.*, 2006] after multiplication with a high-resolution solar spectrum [*Dobber et al.*, 2008]. A Chebyshev expansion combined with a look-up-table is used to perform the convolution with the OMI slit function in an efficient manner. A typical OMI averaging kernel is graphically displayed in Figure 1, revealing that ozone structures in the stratosphere (lowest pressures) are captured well whereas in the troposphere one cannot distinguish between one level and another. The surface underneath the atmosphere is considered to be a Lambertian reflector and has an initial value taken from the OMI surface albedo climatology [*Kleipool et al.*, 2008]. Depending on a threshold value for the cloud fraction, taken from the OMI Cloud Fraction and Height algorithm (OMCLDO2) based on O2-O2 absorption, either the surface albedo or the cloud fraction or cloud albedo is fitted. Fitting the cloud albedo provides the algorithm with more freedom to deal with optically thick clouds that cover the entire pixel. Stray light is fitted separately in the two spectral channels by minimizing the signature of Fraunhofer features in the fit residual. The measurement errors used in optimal estimation are taken from the Level-1B product. The degrees of freedom of the signal (DOF or DFS: the number of independent pieces of information that is retrieved from the reflectance spectrum, taking into account the noise of the signal) of 6–7 is not large enough to determine the ozone amount for all of the 18 layers used here. A-priori ozone profiles are taken from the McPeters-Logan-Labow climatology which varies with latitude and month [*McPeters et al.*, 2007]. To avoid propagating unphysical structures arising from climatological uncertainty, the a-priori profiles are given a constant relative variability and a correlation length of 6 km. Except for ozone hole conditions an a-priori variability of 20% is assumed for all latitudes and altitudes. Ozone hole conditions are assumed to occur for latitudes south of 50°S during the months of August through December. The variability is then 60% for altitudes between 21 km and 50 km and 30% for all other altitudes, and the correlation length is also 6 km. In optimal estimation the retrieval is constrained by the measured data, normalized by the measurement error, and subject to the a-priori statistics of the atmosphere. As a result the retrieved profile will not differ too much from a climatological average, unless forced by the measured radiance. The ozone profile is given in terms of the layer-column

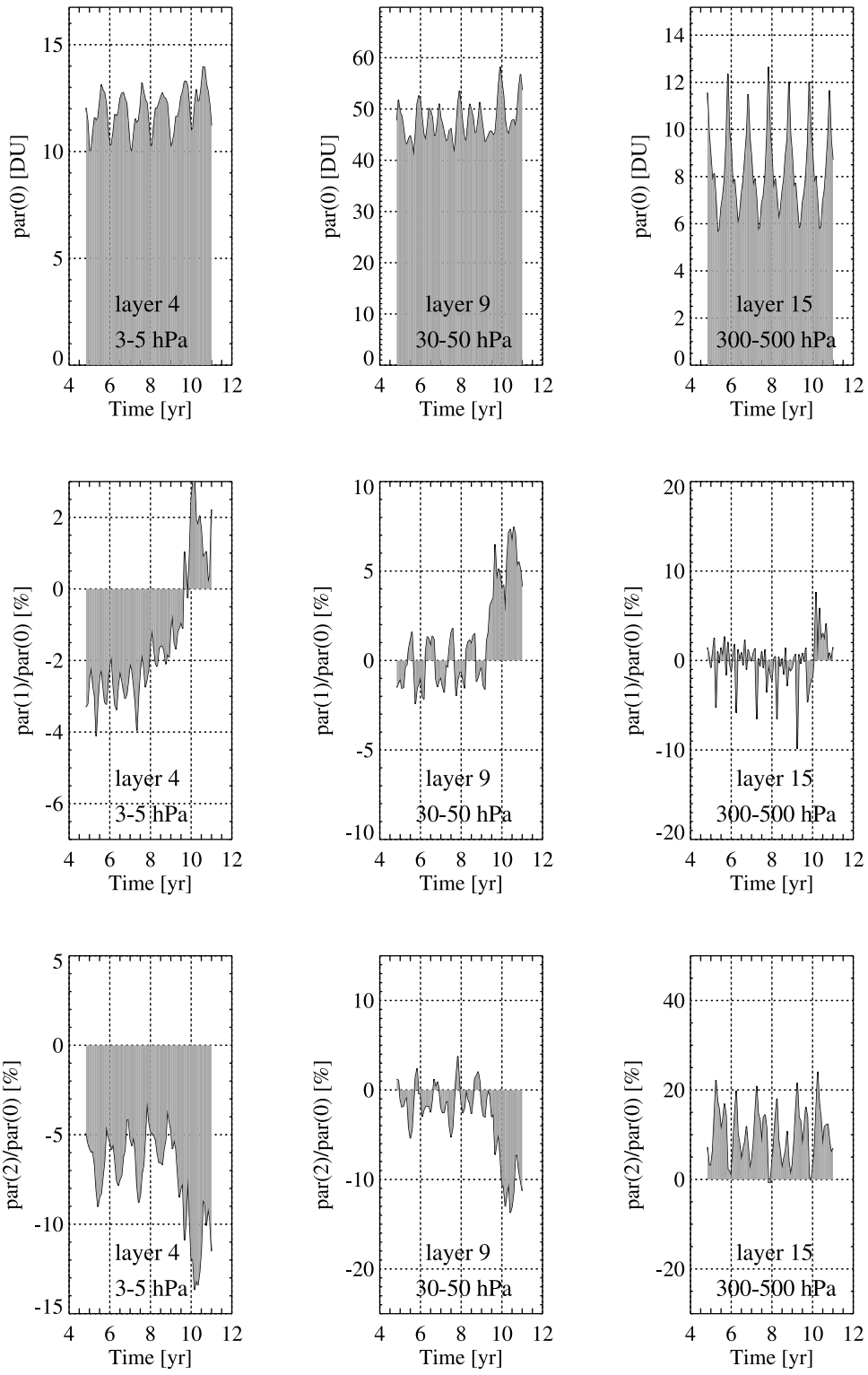


**Figure 3.** Polynomial coefficients P0 [DU], P1/P0 [%] and P2/P0 [%] for selected pressure layers (see insets) plotted against the OMI mission duration for the orbit phase range 153°–162°. *x* axis numbers indicate years of this millennium.

of ozone in DU for an 18-layer atmosphere ranging from surface pressure to 0.3 hPa. The operational algorithm works with the logarithm of the volume mixing ratio (LOG(VMR)) per layer rather than with the VMR itself. This ensures positive values for the retrieved VMR and acts as a constraint on the solution. Current technical limitations on calculation time and data storage compel us to process only 20% of the available pixels hence four out of five measurements in the

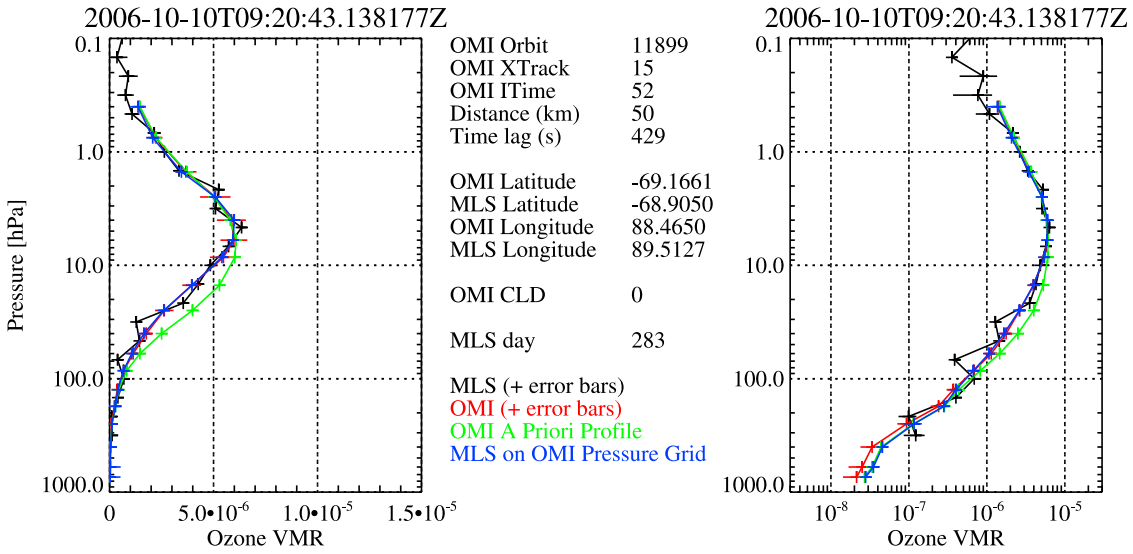


**Figure 4.** Matching single OMI and MLS ozone profiles on a logarithmic pressure scale (*y* axis) and on a (left) linear and (right) logarithmic volume mixing ratio scale (*x* axis). The legend reports the numbers characterizing the collocation.

flight direction are skipped. OMI Level 2 data are stored in the HDF-EOS data format containing basic trace gas abundances and geophysical information plus a wealth of auxiliary information characterizing the atmospheric conditions under which the retrieval was performed and information on the retrieval proficiency. The OMO3PR data set version 003 was publicly released on the 9th September 2009 and can be obtained from the NASA Goddard Earth Sciences (GES) Data and Information Services Center (DISC), home of the GES Distributed Active Archive Center (DAAC). Please visit http://disc.sci.gsfc.nasa.gov/Aura/data-holdings/OMI/index.shtml for more information, including the README [OMI README] and Product Specification files for all OMI data products, where data quality flagging is described in detail. ([OMI README] Please read the README file of this data product carefully prior to use. OMI README files can be found on http://disc.gsfc.nasa.gov/Aura/OMI/.)

## 5. Error Budget Discussion

[6] There are multiple sources of error/uncertainty for the retrieved ozone profile. Errors due to measurement noise, the uncertainty in the a-priori ozone profile, and the smoothing error are covered by the error estimate provided by Optimal Estimation and are quantified by the a-posteriori error covariance matrix employed in this study. However, there are other error sources that are in part difficult to quantify and during development of the algorithm a large number of tests have been performed to obtain an understanding of these error sources. The most important error source appears to be spectral stray light. Some of the light detected at a certain wavelength (detector position) is comprised of light at other wavelengths arriving at the detector through internal reflections and light scattering inside the instrument caused by optical imperfections. A stray light correction algorithm has been developed but does not sufficiently correct for stay light because features corresponding to solar Fraunhofer lines are still present in the residue of the spectral fit. The amplitude of these features depends on the viewing direction, the solar zenith angle, the wavelength range involved and the cloud fraction of the ground scene, which makes it difficult to quantify. To deal with stray light, *Liu et al.* [2010a] apply a soft calibration scheme to OMI level-1B data, minimizing the difference between measured and modeled radiances, in the latter employing ozone profiles obtained from the MLS instrument on board of EOS-Aura. However, we have chosen to fit stray light separately in the UV1 and UV2 channels assuming a low order polynomial in the wavelength for the stray light. This results in a reduction of the amplitude of the Fraunhofer features the residue of the fit by a factor of 2–3 and an improvement in the agreement with MLS ozone profiles. In particular the systematic structures as seen in differences with MLS profiles significantly reduce in amplitude. Quantification of the remaining stray light error, apart from the validation study reported in this paper, is difficult. Based on numerical experiments with different assumptions on the polynomial that is used in the stray light fit, it is expected that a 10% error can remain for the (upper) stratosphere and 30% for the lower stratosphere and troposphere.

[7] There are other sources of errors, such as the absorption cross sections of ozone that are used, the simple Lambertian cloud model that is located at a pressure level derived from O2-O2 absorption near 477 nm, approximations used when correcting for rotational Raman scattering, the use of homogeneous layers when solving the radiative transfer problem (for multiple scattering only), interpolation errors in the correction factor for the polarization look-up table, not accounting for absorbing aerosols, the use of 6 streams instead of 8 streams in the radiative transfer calculations, the use of a Lambertian surface instead of a bidirectional surface when accounting for surface reflection. Estimates obtained from numerical experiments, some of which are reported in the OMI Algorithm Theoretical Basis Document (ATBD), all suggest that the stray light error dominates, even after comprehensively fitting for stray light. As stray light remains inadequately quantified, it is not possible to provide a com-

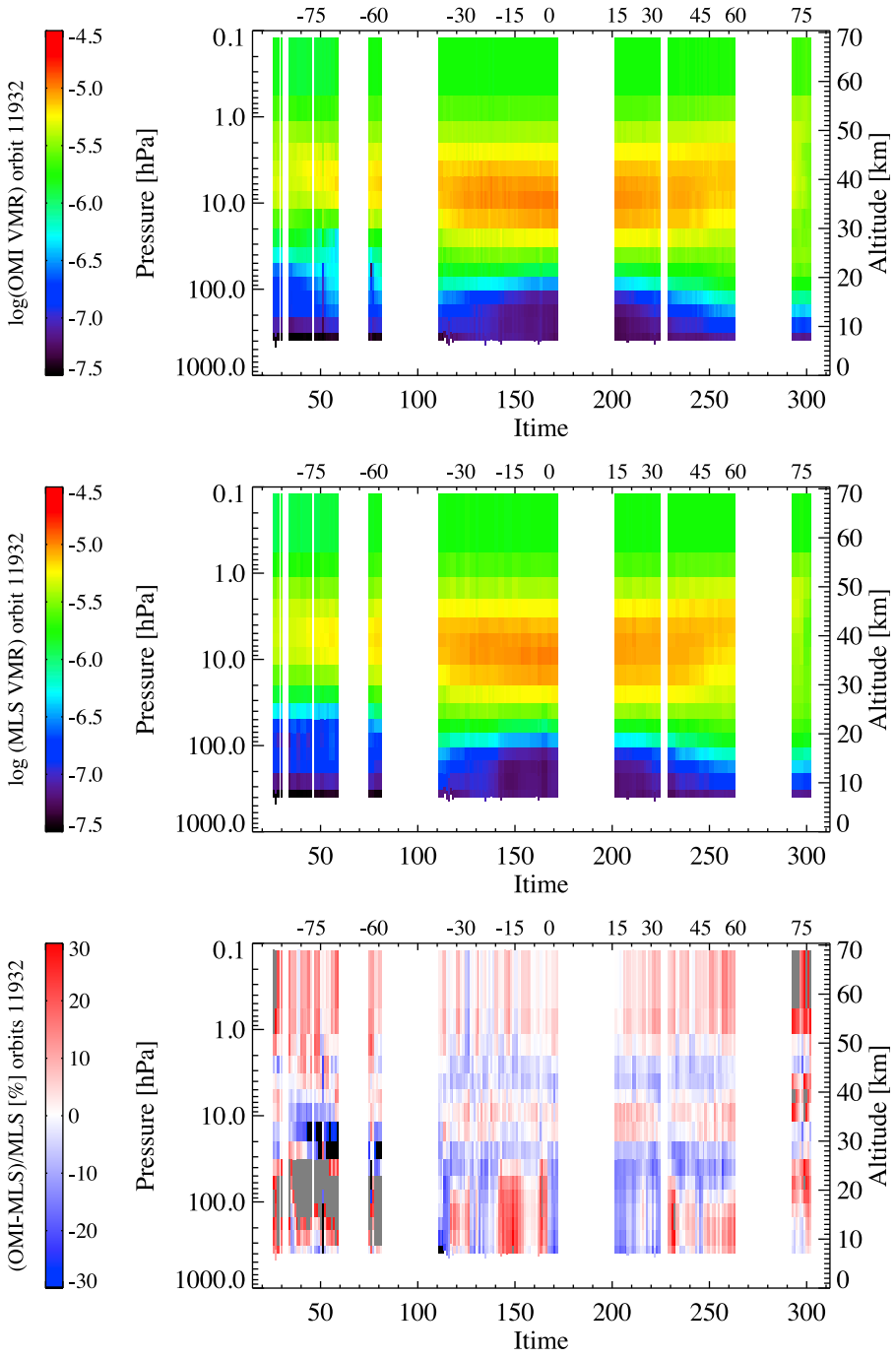


**Figure 5.** Curtain plot of one orbit (12 October 2006, orbit 11932) of (top) OMI, (middle) MLS and (bottom) OMI-MLS collocated profiles. Vertical profiles expressed in LOG(VMR) are plotted against Itime denoting time in units of 10 s (Itime = 329 captures the day-side orbit of Aura). The top axis of each plot also contains indicators for latitude. Relative differences expressed in percentage are plotted against Itime. Data gaps are caused by stringent data filtering.

plete error budget that is independent from the validation studies reported here.

## 6. OMI Row Anomaly

[8] Since June 2007 certain cross track positions in the OMI data are affected by the so-called 'row anomaly'. This anomaly affects all wavelengths for a particular viewing direction of OMI, for example, when there is much less or much more signal detected than nominal over an extended period of time for a partial or full orbit. An OMI viewing direction corresponds to a binned row on the CCD detectors hence the term 'Row Anomaly'. Which rows are affected and to what extent varies strongly with time. The anomalies are currently under investigation to examine whether corrections for the effects can be implemented in the Level-1B radiance

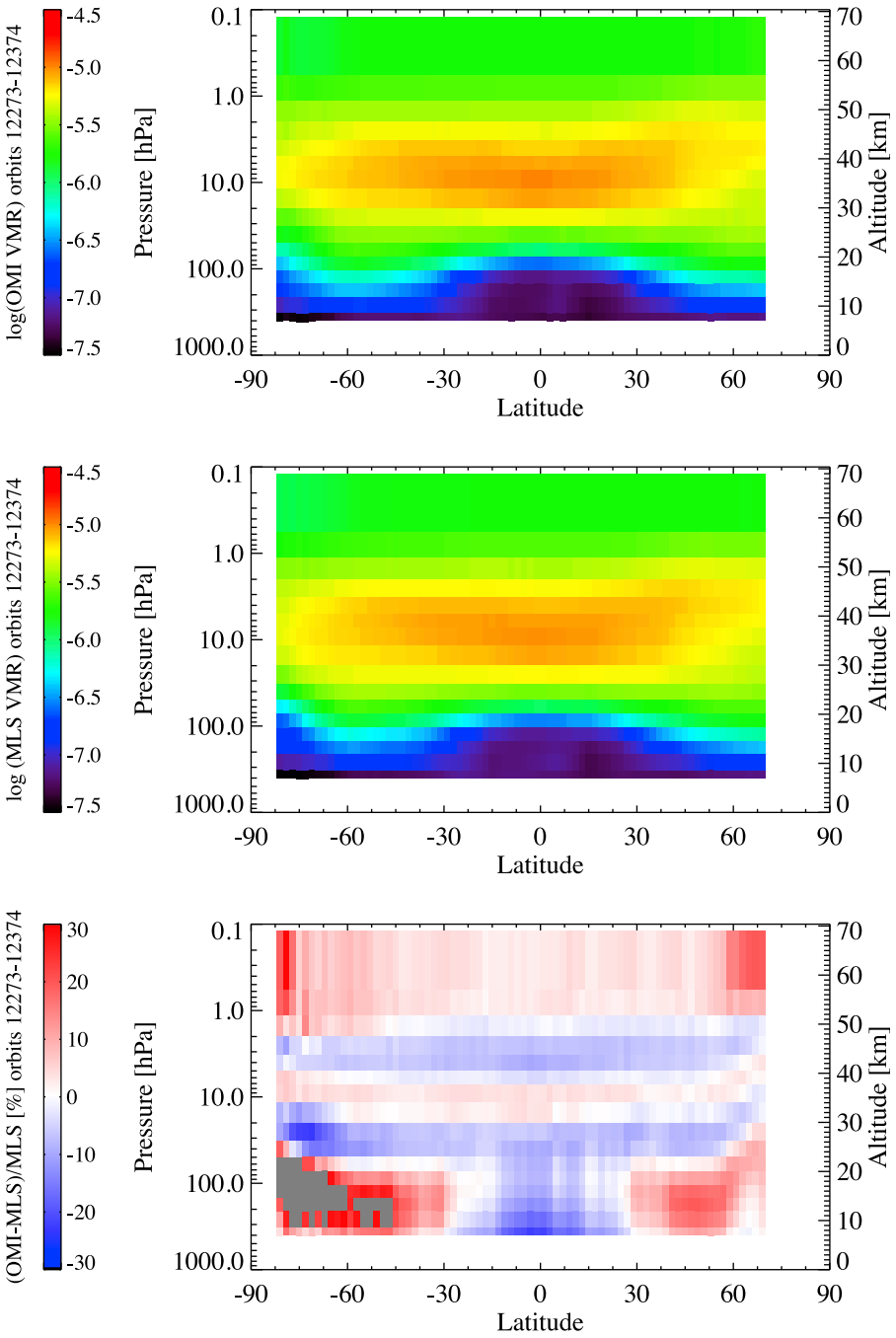


**Figure 6.** Curtain plot of averaging one week of data (6–12 November 2006, week 45, orbits 12273–12374) of (top) OMI, (middle) MLS and (bottom) OMI-MLS collocated profiles. Vertical profiles expressed in LOG(VMR) are plotted against latitude. Relative differences are expressed in percentage.

data. Please visit the OMI product webpage (http://www.knmi.nl/omi/research/product/) and the detailed technical information webpage (http://www.knmi.nl/omi/research/product/rowanomaly-background.php) for information on the row anomaly. At the moment no corrections have been implemented in the operational Level-1B and Level 2 data. Affected Level-1B and Level-2 data has been flagged and it is recommended to use the XTrackQualityFlag for filtering bad data. All values other than '0' indicate affected data. When the row anomaly comes into play from May 2008 onwards and more abruptly from January 2009 onwards, the changes to the retrieved ozone profiles in the affected rows are abrupt. Retrieved ozone columns per sub-layer differ strongly from climatology and profiles appear unphysical. Furthermore, the Reflectance Cost Function, i.e., the $\chi$^2 of fit, obtains values > 50 while nominally its value ranges between 0 and 5. In fact, the settings of the XTrackQualityFlag flag originating from the analysis of Level-1B data have been confirmed using the operational ozone profile data here under investigation. Thus, when respecting the XTrackQualityFlag flag, the row anomaly has no effect on the derived profile products;

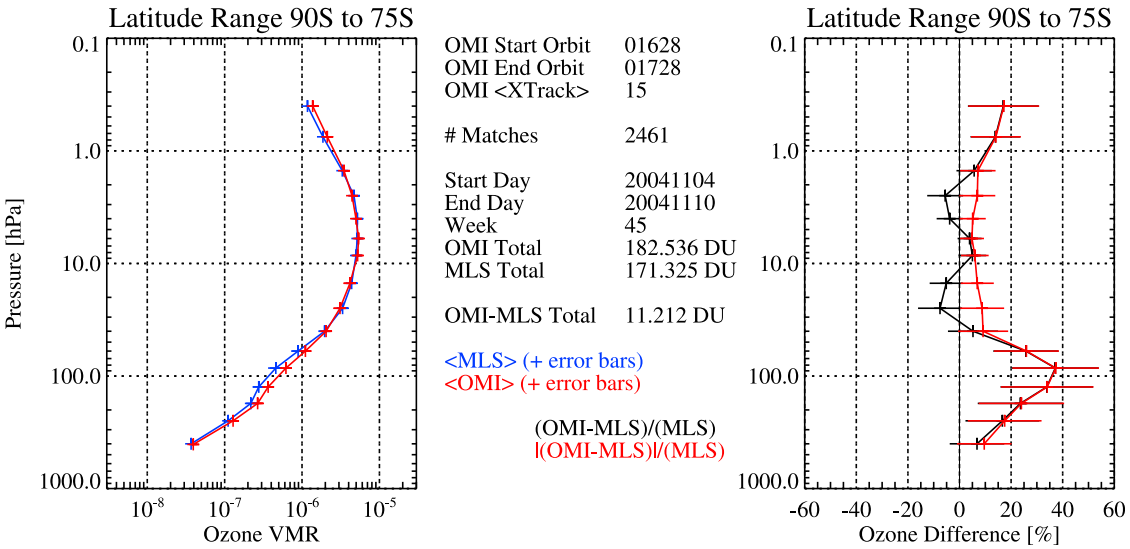


**Figure 7.** (left) Average profile and (right) relative difference of a week of OMI and MLS ozone profiles collocated over Antarctica [90S-75S]. The legend reports the numbers characterizing the time frame and statistics of this collocation.

it simply reduces the amount of data available by reducing the daily geographical coverage of the OMI data.

## 7. OMI Ozone Profile Data Quality Analysis

[9] To test the consistency of the OMI ozone profile data, we calculated monthly zonal cross track averages of each of the 18 sub-columns. The averages are calculated for 9° orbit phase bands where orbit phase is defined as 0° (0.00) at the spacecraft midnight point, 90° (0.25) at the southern hemisphere terminator, 180° (0.50) at the spacecraft midday point and 270° (0.75) at the Northern hemisphere terminator. Hence orbit phase runs from 90° to 270° (0.25–0.75) on the dayside portion of the ascending EOS-Aura orbit. An example is shown in Figure 2, portraying the results for 3 selected pressure levels for the orbit phase range 153°–162° for October 2004. The pressure layers represent the upper and lower stratosphere and troposphere and this orbit phase range covers part of the southern hemisphere below the equator. Here we use data with cloud fractions below 20% and filtered for the ProcessingQualityFlags and XTrackQualityFlag flags. Ideally these plots should show flat lines indicating that independent of the OMI viewing angle the same amount of ozone is retrieved on average per sub-column during that month. To parameterize the cross track dependence we match a second order polynomial function to the data on a normalized $x$ axis, ranging from [−1,1] on which all three polynomial coefficients have the dimension of Dobson Units [DU]. In

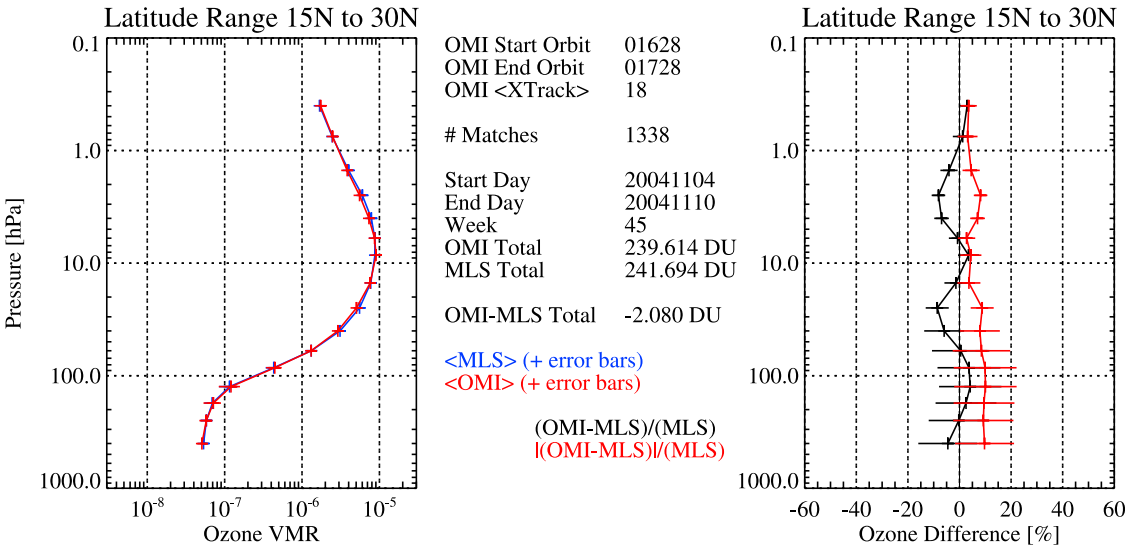


**Figure 8.** (left) Average profile and (right) relative difference of a week of OMI and MLS ozone profiles in the northern sub-tropics [15N–30N]. The legend reports the numbers characterizing the time frame and statistics of this collocation.

Figure 3 we plot the dependence of the coefficients against the OMI mission duration for the orbit phase range 153°–162°. The 0th order coefficient reveals the seasonal and natural changes of the all-row-averaged ozone concentration for each pressure level. The 1st order coefficient is normalized to the 0th order polynomial coefficient to indicate the relative contribution of the linear term to the sub-column. In the stratosphere, most variations fall between the range −5% to +5%. In the troposphere the linear term contributions are more substantial. Particularly interesting is the slow but continuous positive trend in level 4 that seems to be ongoing since the beginning of the OMI data record. The 2nd order coefficient is normalized to the 0th order coefficient to indicate the relative contribution of the quadratic term to the sub-column. The 2nd order term is almost a factor of 2 larger than the 1st order term as is confirmed by the symmetric smile shaped curve rather than a linear tilt in the plots of Figure 2. For most pressure levels the 2nd order term values change more irregularly with time of year compared to the lower order terms. Many levels tend to show fast switches in the sign of the 'smile' with time. In the stratosphere, most variations fall between the range −15% to +10%. In the troposphere the quadratic term contributions are much more substantial, up to 40%. Overall these results indicate that most layers of the OMI ozone profile have a substantial cross track dependence that should be confirmed and quantified by validation where the second order term is most significant. Figure 3 also shows that for the time frame October 2004–December 2008 the OMI data is of high quality and unaffected by the occurrence of the row anomaly. This situation changes slightly after January 2009 and more strongly after July 2009. Only above orbit phase of ~210° (0.59) does the row anomaly affect other rows than those reported on our information web pages. Beyond January 2009 we recommend that users not use OMI ozone profile data for scientific purposes above the orbit phase of ~210° (0.59).

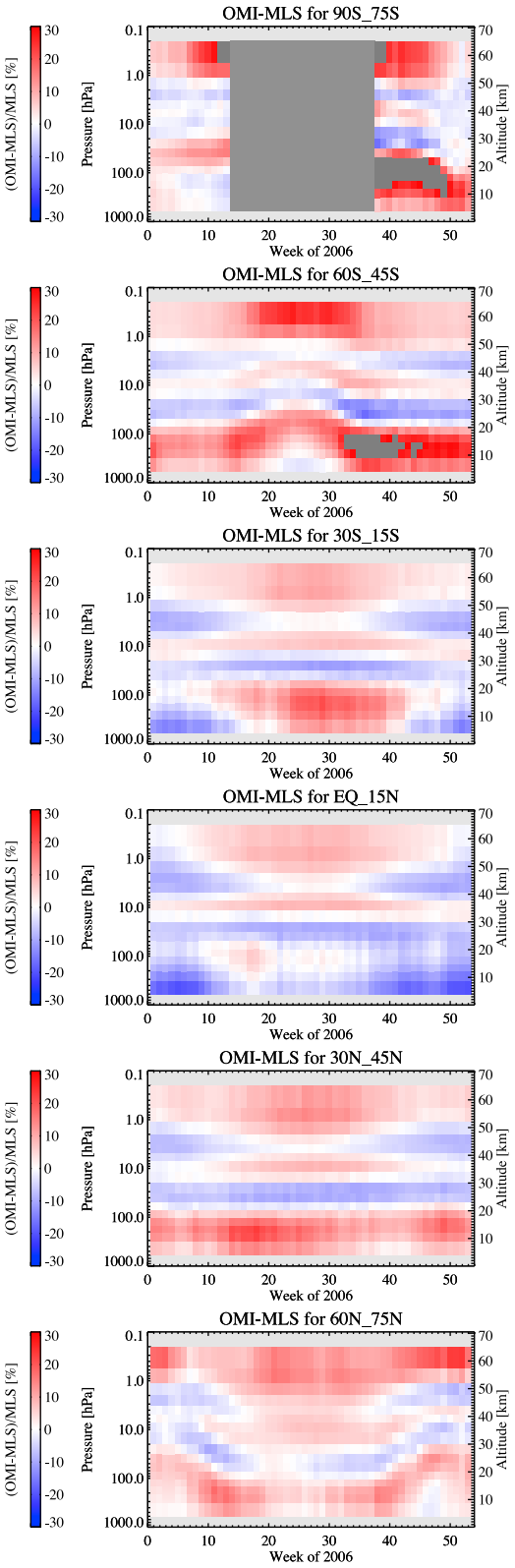


## 8. Validation Against MLS Aboard NASA EOS-Aura

[10] The forward looking Microwave Limb Sounder (MLS) co-flying with OMI aboard the NASA EOS-Aura platform measures the naturally occurring microwave thermal emission from the limb (edge) of the Earth's atmosphere to remotely sense vertical profiles of many atmospheric trace gases, temperature, pressure, and cloud ice [*Waters et al.*, 2006]. MLS takes measurements along-track and performs ~240 limb scans per orbit with a footprint of ~6 km across-track and ~150 km along-track. Tracking of the changes in the stratospheric ozone layer from about 15 to 50 km altitude as well as the total ozone column down to the ground are important goals for all the EOS-Aura satellite teams. The ~3500 daily MLS ozone profiles obtained both day and night are a very useful component of this research and have proven to be of very high quality as revealed by validation exercises against ground based balloon soundings and other space born limb sounders [*Froidevaux et al.*, 2006, 2008; *Jiang et al.*,

**Figure 9.** Average of OMI and MLS ozone profile relative differences calculated and plotted per week of data for selected latitude bands for the year 2006. Results for 2006 are typical for the results obtained during other years. Dark gray areas (covering all altitudes) denote an absence of OMI data due to the absence of sunlight for that season and hemisphere combination. Black and Grey data points denote out-of-scale positive and negative values, respectively.

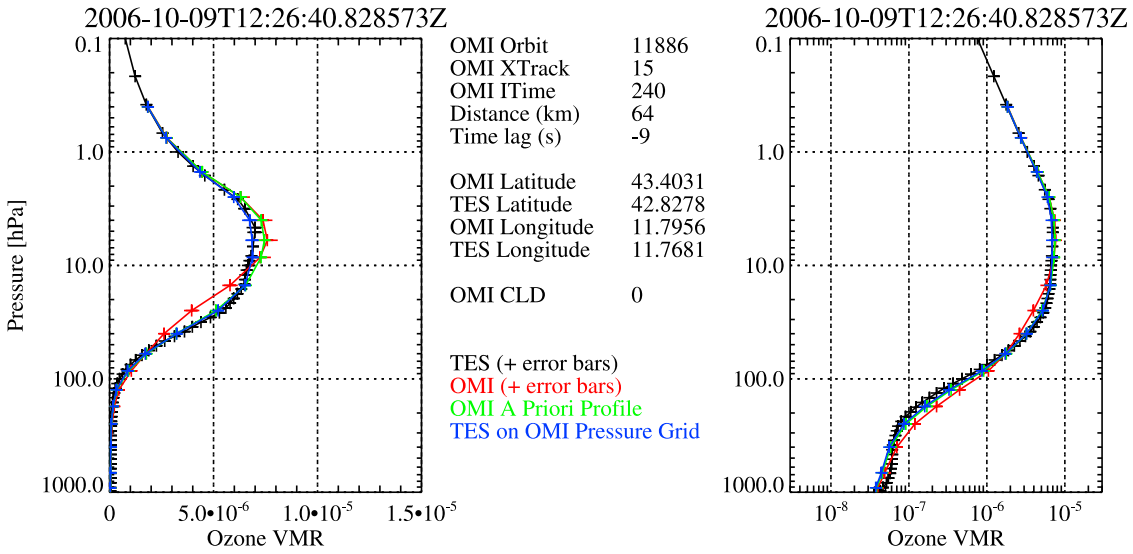


**Figure 10.** Matching single OMI and TES ozone profiles on a logarithmic pressure scale ($y$ axis) and on a (left) linear and (right) logarithmic volume mixing ratio scale ($x$ axis). Figure 10 (left) highlights the stratospheric ozone profile whereas Figure 10 (right) also shows details of the troposphere. The legend reports the numbers characterizing the collocation.

2007; *Livesey et al.*, 2008]. For comparison of individual OMI MLS ozone profiles we treat the MLS data as "true values" because the stratospheric component of the MLS ozone profiles have much lower uncertainties and higher vertical resolution than the OMI profiles but much coarser horizontal resolution and sampling. MLS data is filtered using data quality flag fields recommended by the MLS team: 'quality' higher than 1.2, 'convergence' less than 1.8, positive 'precision' values and 'status' equal to zero. The MLS vertical resolution is estimated to be 2.7–3.0 km from the upper troposphere to the middle mesosphere and the vertical range recommended for using MLS data is 0.02–215 hPa. Here we employ MLS ozone profile data labeled L2GP-O3 of version 2.2 as publicly available from the NASA Goddard Earth Sciences (GES) Data and Information Services Center (DISC).

[11] EOS-Aura flies in orbit at 7.5 km per second ground speed and OMI observes the same air mass in nadir roughly 7 min later than MLS in limb yielding a temporal bias of ~420 s. Spatiotemporal collocation criteria are to find ozone

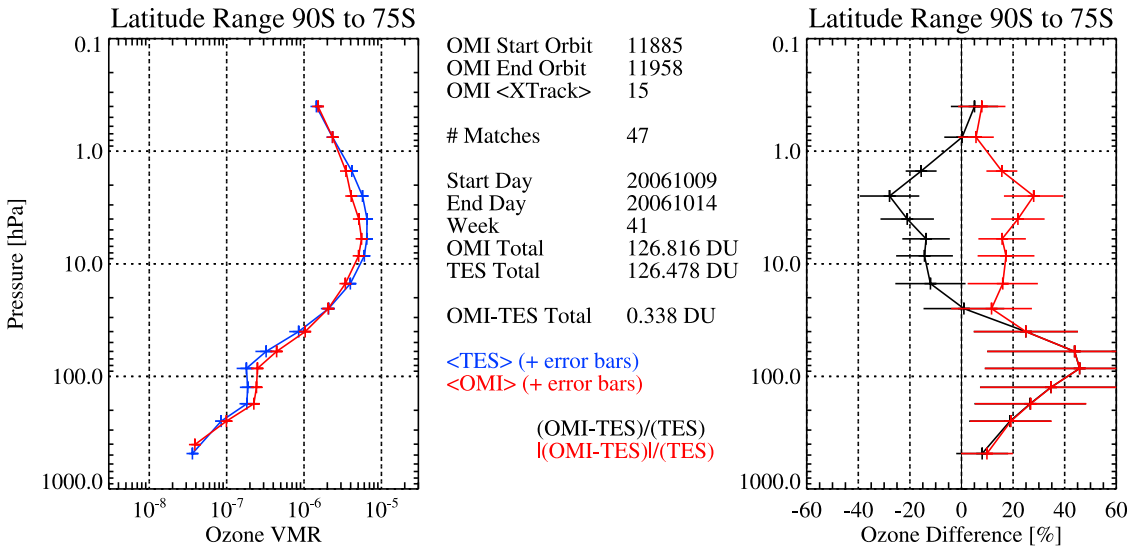


**Figure 11.** (left) Average profile and (right) relative difference of a week of OMI and TES ozone profiles collocated over Antarctica [90S-75S]. The legend reports the numbers characterizing the time frame and statistics of this collocation.

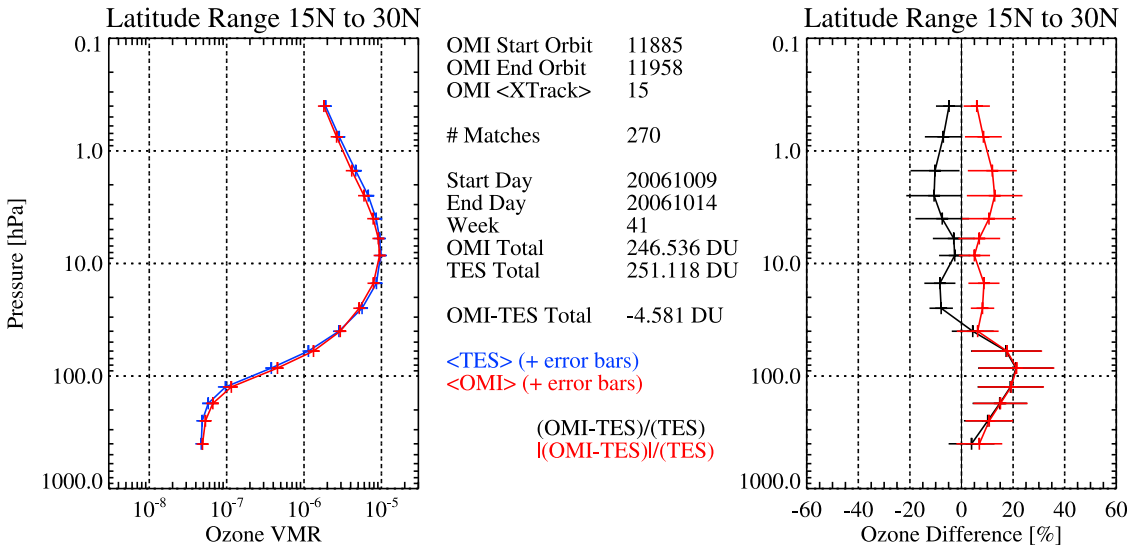


**Figure 12.** (left) Average profile and (right) relative difference of a week of OMI and TES ozone profiles in the northern sub-tropics [15N-30N]. The legend reports the numbers characterizing the time frame and statistics of this collocation.

profile pairs within 150 km and within 120 s around this bias. In the polar regions the air mass sampled by MLS coincides with OMI nadir cross track position 14 as the rotational velocity of the Earth's surface is near zero. However, at the equator this coincidence shifts to OMI cross track position 18 due to the rotational velocity of the Earth's surface and atmosphere where we ignore the impact of local winds. Thus we need a spatial bias correction as a function latitude because the air mass first seen by MLS rotates away from OMI during the temporal difference between Limb and Nadir sampling on the sun-synchronous ascending polar orbit of EOS-Aura. Therefore we appropriately adjust the OMI cross track position coincident with the MLS ground track between 14 and 18 integer wise as a function of latitude. Collocated MLS profiles are converted to the OMI pressure level grid incorporating the OMI averaging kernels and the ozone profile a-priori information following *Liu et al.* [2010b]. First MLS volume mixing ratios are converted to Dobson Units per MLS pressure layer and accumulated to obtain the MLS cumulative sum with pressure. This array is linearly dispersed on the coarser OMI pressure level grid to an initial MLS ozone profile. Subtracting the OMI a-priori profile, matrix multiplication with the OMI averaging kernel and again adding the OMI a-priori profile to this initial profile yields the OMI weighted MLS profile in Dobson Unit per OMI pressure layer labeled MLSOMIak following;

$$MLSOMIak = OMIap + OMIak\#(MLSOMI - OMIap),$$

where *OMIap* is the OMI a-priori, *OMIak* is the OMI averaging kernel, *MLSOMI* is the initial MLS ozone profile interpolated on the OMI pressure level grid. Application of the OMI averaging kernels removes the smoothing error of bringing MLS data to the OMI pressure grid, where the smoothing error is considered to be a major contributor to the error budget [*Liu et al.*, 2010b]. Both OMI and collocated OMI weighted MLS profiles are then converted to volume mixing ratios. Since the MLS averaging kernels are much more narrow than the OMI averaging kernels, weighting the OMI vertical ozone profiles with the MLS averaging kernels was not performed. When comparing OMI to MLS we do not filter for clouds. The method described here, in which MLS serves as the first example, follows *Rodgers and Connor* [2003] who presented a general method to compare measurements from two satellite instruments with different averaging kernels, by smoothing the retrievals from the instrument with higher vertical resolution using the averaging kernels of the instrument with lower vertical resolution. This method is generally applied to all correlative data used in this study, being satellite data or balloon ozonesonde data, as OMI data is presented on the most coarse pressure grid of all.

[12] An example of a single profile match of OMI and MLS under ozone hole conditions is plotted in Figure 4 for the 10th of October 2006. The OMI ozone profile deviates significantly from the a-priori profile at low ozone concentrations although the error bars are small compared to the excursions away from the a-priori. A careful examination of the climatology revealed that at some latitudes at certain times of the year the ozone profile climatology was comprised of very few balloon sonde profiles with a small spread that limited the retrieval in its excursions away from the climatological mean. Setting the a-priori variability to much larger values than prescribed by the climatology allows the retrieval to use the available data to its fullest and to accurately converge to a scientifically sound solution that strongly deviates from climatology as shown in Figure 4. It also shows that the climatology does not statistically represent the true atmosphere. Another view on matching OMI to MLS is presented in Figure 5 where we depict all collocated pairs and their relative difference for one full orbit of data, typically yielding ~200 matches. In the upper two panels of Figure 5 the OMI and MLS ozone profiles are expressed in LOG(VMR) to highlight features in the lower stratosphere and troposphere. The profiles are plotted against the OMI Itime parameter denoting flight time in units of 10 s. The latitude accompa-

nying the profiles is printed above each of the curtain plots for every 15°. The ascending OMI orbit starts at Itime = 0, spots the southern terminator at Itime = 15, passes solar midday at Itime = 165, spots the Northern terminator at Itime = 314 and ends at Itime = 329. MLS tends to show a deeper ozone hole and OMI reveals much more spatial detail of the stratospheric ozone abundance. In the lower panel of Figure 5 the OMI to MLS relative differences are shown, following 100%*(OMI-MLS)/MLS. Persistent structures varying with latitude seem to follow the tropopause.

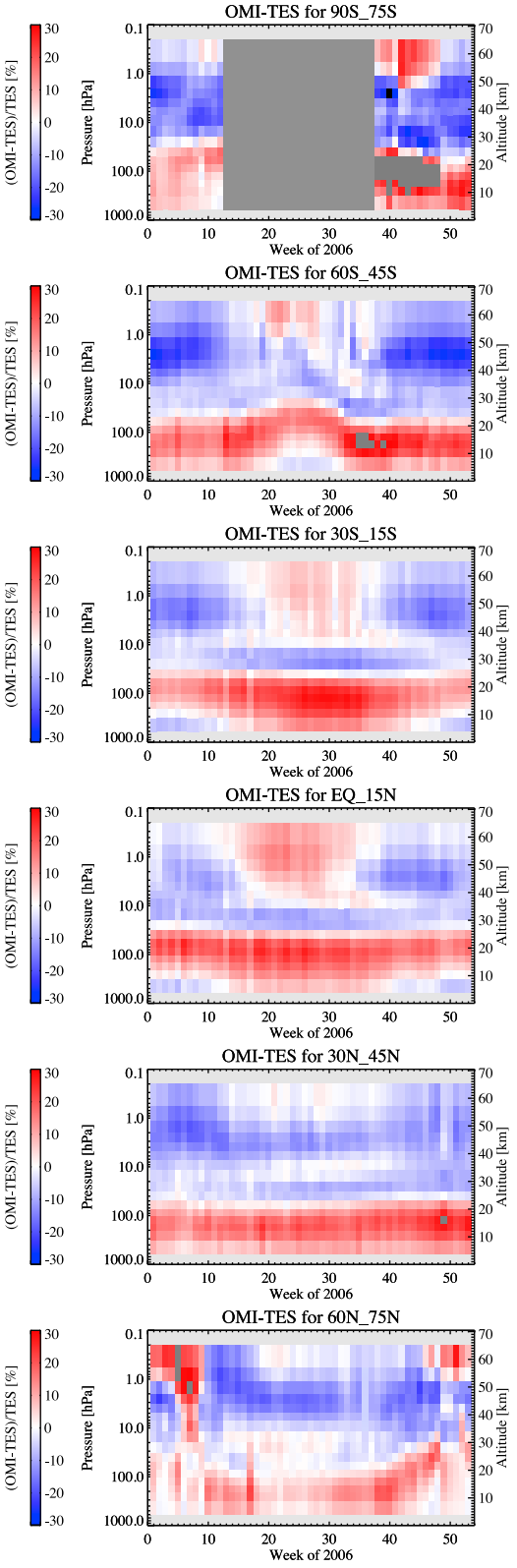


**Figure 13.** Average of OMI and TES ozone relative profile differences calculated and plotted per week of data for selected latitude bands for the year 2006 along the lines of Figure 9. Results for 2006 are typical for the results obtained during other years. Dark gray areas (covering all altitudes) denote an absence of OMI data due to the absence of sunlight for that season and hemisphere combination. Black and Grey data points denote out-of-scale positive and negative values, respectively.

[13] Statistics of collocated profiles derived per week range between 10500 and 17500 matched pairs, or 116–194 matches per 2° latitude bin. Examples are shown in Figure 6 for week 41 of 2006. The OMI and MLS ozone profiles are again expressed in LOG(VMR) to highlight features in the lower stratosphere and are plotted here against latitude. In the lower panel of Figure 6 the average OMI-MLS differences are shown. Although at first glance the two upper images are remarkably similar, the OMI-MLS difference shows persistent structures with pressure/altitude substantiating the persistence of the features first observed in Figure 5. In the tropics OMI significantly overestimates tropospheric ozone concentrations with respect to MLS. Everywhere else the situation is reversed. At the highest southern latitudes the differences are most pronounced, changing from beyond +30% to near −30% with altitude, confirming earlier observations that MLS 'sees' a much deeper ozone hole. Most of the structure seen in Figure 6 moves with season hence it is persistent with solar zenith angle or orbit phase, but not with latitude.

[14] Statistics of collocated profiles and their differences calculated per week are binned to 15 degree latitude bands to study temporal evolution of zonal bands. Examples are shown in Figure 7 for Antarctica (worst case) and Figure 8 for the northern sub-tropics (best case) for week 45 of 2004. Statistics per week per latitude band range between 1500 and 2500 matches. The error bar plotted per data point reflects the statistical spread ($1\sigma$). Over Antarctica OMI tends to overestimate the ozone concentrations above 50 hPa with respect to MLS whereas at higher altitudes the differences are much smaller. Figure 7 (right) shows that differences are limited to [−15%, +35%]. In the northern sub-tropics differences are limited to [−15%, +10%] and the best match is obtained in the tropics. Plots for other time frames and latitude bands all show the persistent character of the OMI-MLS difference plot where the altitudes of the crossings with the zero difference line depends on season and latitude. Finally, in Figure 9 we plot the OMI-MLS difference averaged for selected latitude band for the entire year 2006. The features highlighted by Figure 9 are typical for all other years of the OMI mission; (i) persistent structures with altitude for all latitudes; (ii) the sign of the differences are often changing with time; (ii) differences are largest under ozone hole conditions; (iii) best results are obtained in the tropics where differences are limited to [−10%,+10%]. Figure 9 shows that with time the latitudinal location of positive and negative features in the OMI-MLS difference changes, they move around with sea-

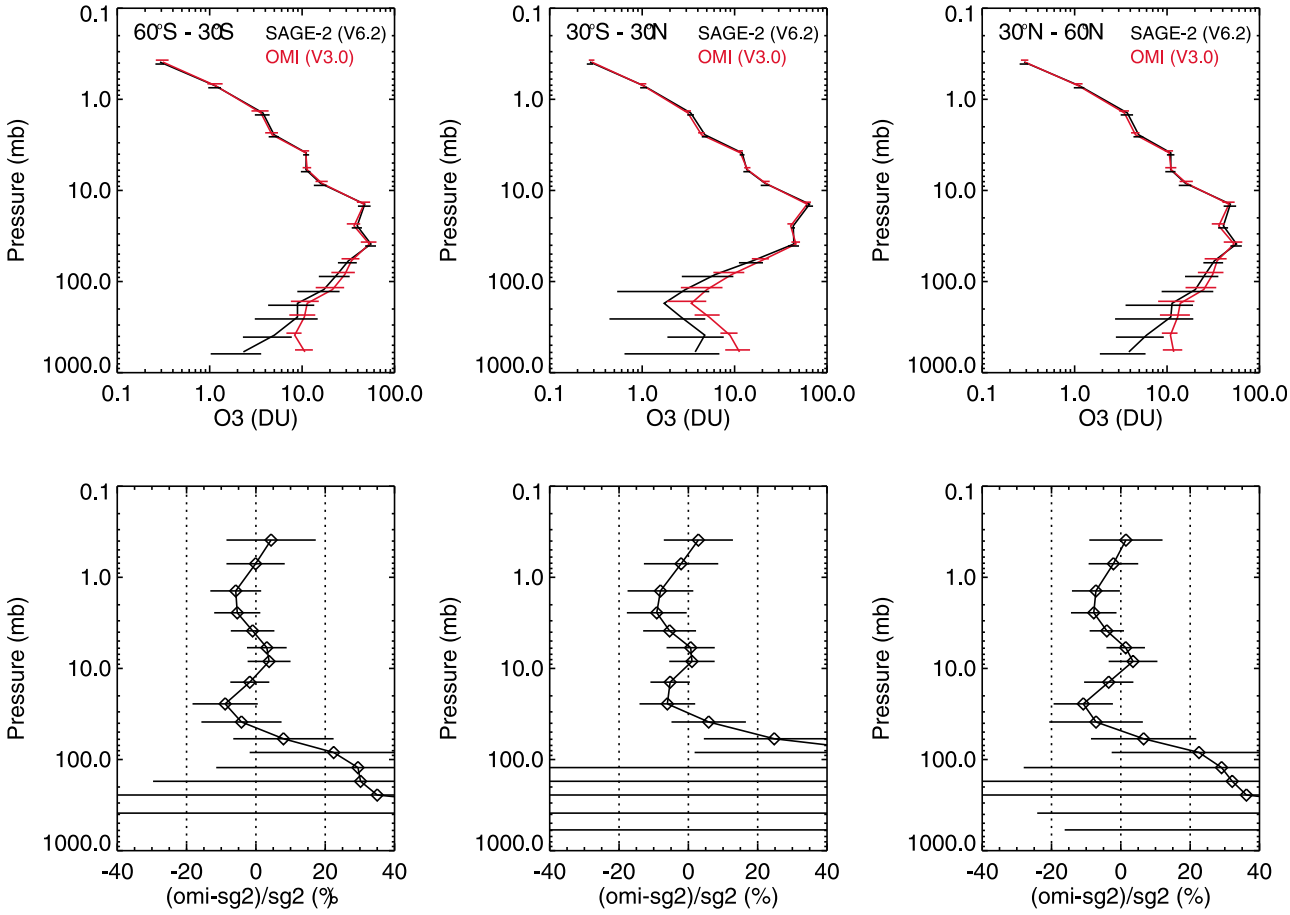


**Figure 14.** (top) Mean ozone profiles from collocated OMI (red) and SAGE-II (black) measurements at three latitude bands, (left) 60S-30S, (middle) 30S-30N, and (right) 30N-60N. (bottom) Corresponding median relative differences and statistical spreads between OMI and SAGE-II. The spread is defined as one half of differences between the 16th and 84th percentiles (see text).

son in weekly plots of Figure 6. Therefore we do not present annual averages of the difference with latitude as this most probably reduces the differences seen per week hence not representing the actual differences.

## 9. Validation Against TES Aboard NASA EOS-Aura

[15] The Tropospheric Emission Spectrometer (TES) is also co-flying with OMI aboard the NASA EOS-Aura platform. TES is a high-resolution infrared-imaging Fourier transform spectrometer that offers a line-width-limited discrimination of essentially all radiatively active molecular species in the Earth's troposphere. Routine standard products from TES include vertically resolved profiles for ozone, carbon monoxide, water vapor, deuterated water vapor and methane. TES nominally operates in nadir mode called the global survey mode. TES takes measurements along-track and performs ~3350 nadir scans per day with a single observation ground footprint of ~5.3 km across-track and ~8.3 km along-track spaced ~180 km apart along-track. TES data is filtered using data quality flag fields recommended by the TES team; the SpeciesRetrievalQuality flag and the ozone profile lapse rate flag (O3_Ccurve_QA) must read '1' for good data. The "master" quality flag SpeciesRetrievalQuality is the culmination of an elaborate set of quality flags as developed for TES data [*Osterman*, 2009]. We exclude cloudy TES profiles by removing data for TES cloud optical depth > 2.0 following Nasser *et al.* (2007) and cloudy OMI profiles by removing data for OMI cloud top pressures < 650 hPa. Profiles with thick high clouds in the field of view are thus removed because they obscure the infrared emission from the lower troposphere and hence greatly reduce the TES sensitivity below the cloud. Excluding cloudy scenes strongly reduces the number of matches obtained per week but ensures we are looking at measured tropospheric ozone profiles rather than the a-priori. Since OMI and TES basically look at the same ground scene it also excludes cloudy OMI pixels hence this comparison can be classified as 'cloud free'. Our OMI-MLS comparisons, which have a more stratospheric focus, can be classified as 'all scenes' as they are not filtered for clouds. In fact, filtering for cloudy scenes in the OMI-MLS comparisons does not yield significant changes in the outcome the comparison. Although the TES ozone profile data points are closely spaced in pressure/altitude, the actual TES vertical resolution, defined as the Full Width at Half Maximum of the averaging kernels, is estimated to range

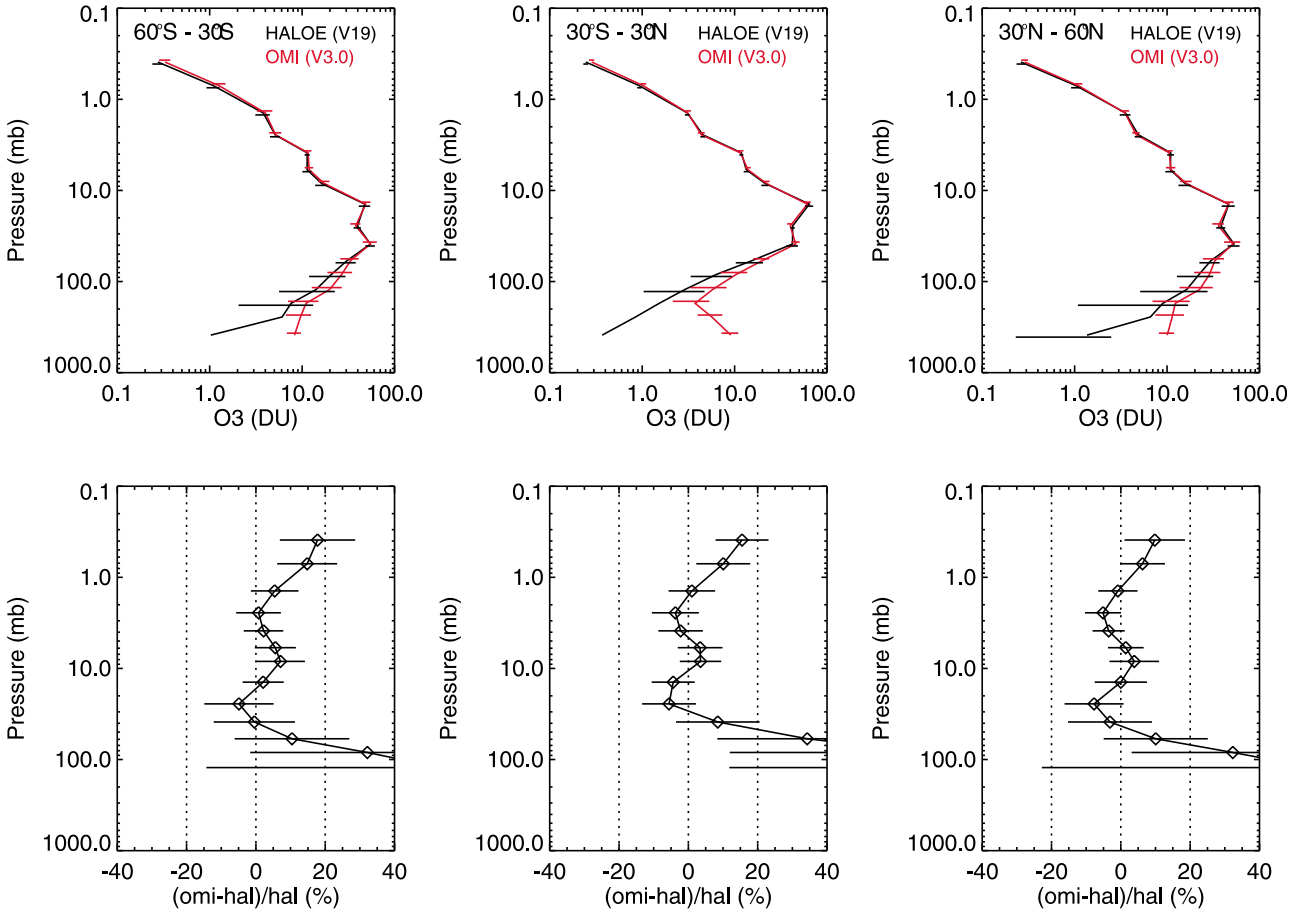


**Figure 15.** (top) Mean ozone profiles from collocated OMI (red) and HALOE (black) measurements at three latitude bands, (left) 60S–30S, (middle) 30S–30N, and (right) 30N–60N. (bottom) Corresponding median relative differences and statistical spreads between OMI and HALOE. The spread is defined as one half of differences between the 16th and 84th percentiles (see text).

from ~5 km in the lower troposphere to ~12 km in the upper stratosphere, respectively, which is comparable to the OMI ozone profile vertical resolution. Here we employ TES nadir ozone profile data as publicly available from the NASA Langley Atmospheric Science Data Center (ASDC) labeled TL2O3N of version F05_07 of the V004 release. The analysis of OMI against TES is performed along the lines of the analysis of OMI against MLS as presented in the previous section. TES and OMI retrievals tend to rely rather strongly on the a-priori data in the stratosphere and troposphere, respectively, and therefore we follow *Zhang et al.* [2010] to correct for the discrepancy that originates from the use of different a-priori profiles by the OMI and TES retrievals. This correction is performed by (i) interpolation of the OMI a-priori profile on the finer TES pressure grid yielding *OMIapTG* and (ii) correcting the TES ozone profile for the difference in TES and OMI a-priori profiles through the TES averaging Kernel yielding *TESapc* following;

$$\ln(TESapc) = \ln(TES) + (I - TESak)\#(\ln(OMIapTG) - \ln(TESap)),$$

where *TES* is the TES profile on the TES pressure grid, *I* is the identity matrix, *TESak* is the TES averaging kernel and *TESap* is the TES a-priori ozone profile, prior to (iii) the interpolation of the TES ozone profile on the coarser OMI pressure grid through the OMI averaging kernel in the same way as we dealt with the MLS data.

[16] A typical example of a good profile match of OMI and TES is plotted in Figure 10 for the 9th of October 2006 where the two satellite instruments agree well. Overall, matched OMI and TES profiles tend to show somewhat larger relative differences than matched OMI and MLS profiles.

[17] In Figure 11 for the Antarctic region and Figure 12 for the northern sub-tropics we show the statistics per 15 degree latitude band of collocated profiles and their differences as calculated for week 41 of 2006, ranging between 31 and 370 matches. The error bar plotted per data point reflects the statistical spread ($1\sigma$). And in Figure 13 we plot the OMI-TES difference averaged per week per 15 degree latitude band for the year 2006 showing the persistent character of the OMI-TES difference plot with altitude. The OMI-TES results differ from the OMI-MLS comparisons in the sense that the positive bias in the troposphere (1000–100 hPa) appears to be more pronounced as well as the persistently negative bias in most of the stratosphere (100–1 hPa). Not correcting for the differences in a-priori profiles results in a misleading positive bias of OMI-TES which is entirely caused by the differences in a-priori profiles. The OMI-TES

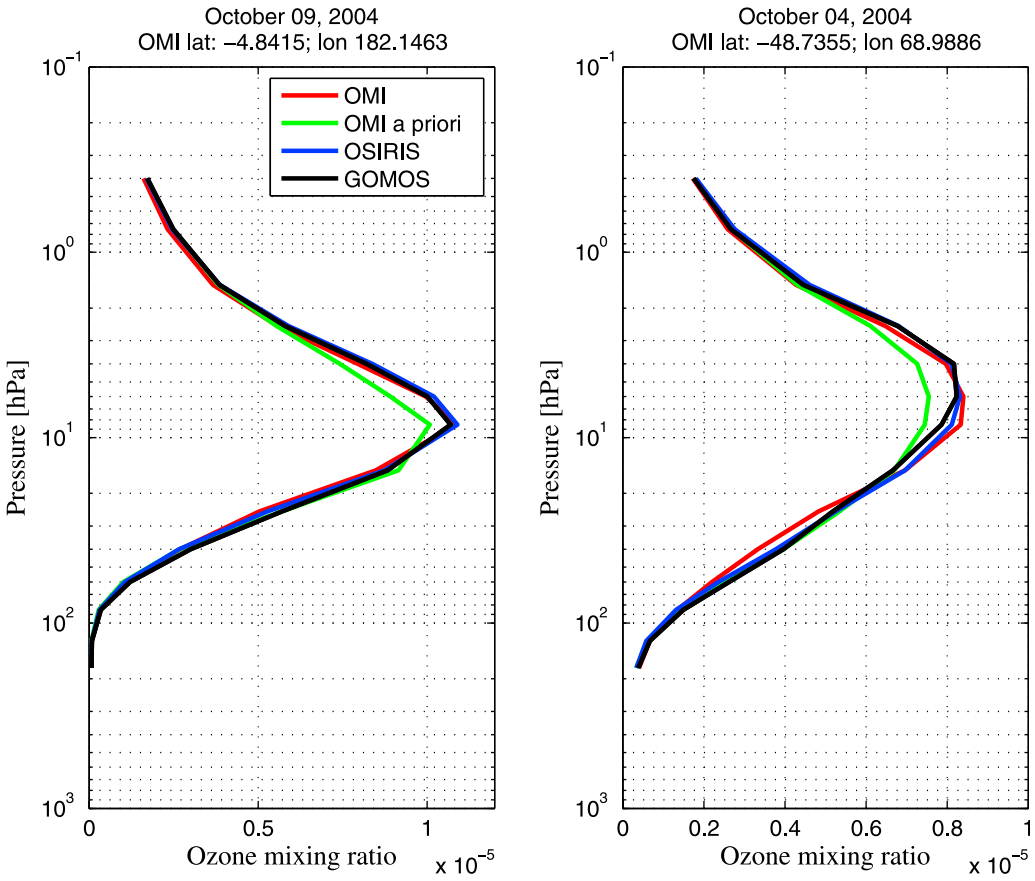


**Figure 16.** Individual ozone profile matches between OMI, GOMOS and OSIRIS on October 9 and 4 of 2004. Temporal collocation of OMI with GOMOS and OSIRIS within 24 h. Spatial collocation of OMI with GOMOS and OSIRIS within 1° × 1° and 5° × 2° degrees in latitude and longitude, respectively.

differences are smallest in the tropics, limited to the range [−20%, +20%] but often better. Over the midlatitudes the differences are larger, in the range [−30%, +30%]. Largest differences are found over the polar regions up to [−60%, +60%]. In all cases these differences are larger than their statistical spread ($1\sigma$). The TES team states that TES is not validated above the height of ozonesondes, about 10 hPa pressure, and recommends not comparing to TES below this pressure because of the sensitivity drop-off and lack of validation (S. Kulawik, NASA JPL, private communication, 2011). Nonetheless, the results of our comparisons look reasonable at pressures below, or altitudes above, this recommended limit.

## 10. Validation Against SAGE-II and HALOE

[18] The Stratospheric Aerosol and Gas Experiment (SAGE-II) instrument employs the solar occultation technique to measure vertical profiles of ozone ($O_3$), nitrogen dioxide ($NO_2$), water vapor ($H_2O$) and aerosol extinctions from its observations at 7 different wavelengths ranging from 0.385 $\mu$m to 1.02 $\mu$m [*McCormick et al.*, 1989; *Cunnold et al.*, 1989]. The SAGE-II observations are taken during satellite sunrise and sunset events from approximately 150 km altitude down to the cloud top providing ~30 profiles each day at a spatial scale of ~200 km. The spatial coverage of all measurements within each day changes slowly in latitude and it takes about 1 month for SAGE-II to provide near global coverage between 80°N to 80°S, depending on season. The SAGE-II instrument provided measurements between October 1984 and August 2005. Similar to SAGE-II, the Halogen Occultation Experiment (HALOE) [*Russell et al.*, 1993] instrument on board of the Upper Atmosphere Research Satellite (UARS) also employs the solar occultation technique to measure trace gases. In contrast to SAGE II, HALOE samples the infrared part of the EM-spectrum between 2.5 microns and 11.0 microns. From the HALOE observations the vertical profiles of ozone ($O_3$), other trace gases and atmospheric temperature and aerosol extinction are retrieved [*Russell et al.*, 1993]. Due to their similar orbit geometry (e.g., ~57 degree inclination, ~600 km altitude), the atmospheric sampling by HALOE is very similar to that of SAGE-II. The HALOE instrument was operated between September 1991 and November 2005 hence the data sets of SAGE-II and HALOE strongly overlap spatiotemporally.

[19] The data sets that we use here are the SAGE-II version 6.2 and the HALOE version 19 ozone vertical profile data sets. Version 6.1 of the SAGE-II ozone vertical profile data set was thoroughly validated by *Wang et al.* [2002] where it showed good agreement against ECC ozonesondes within ~10% over its entire vertical range from the upper stratosphere down to the tropopause. Relative to ECC

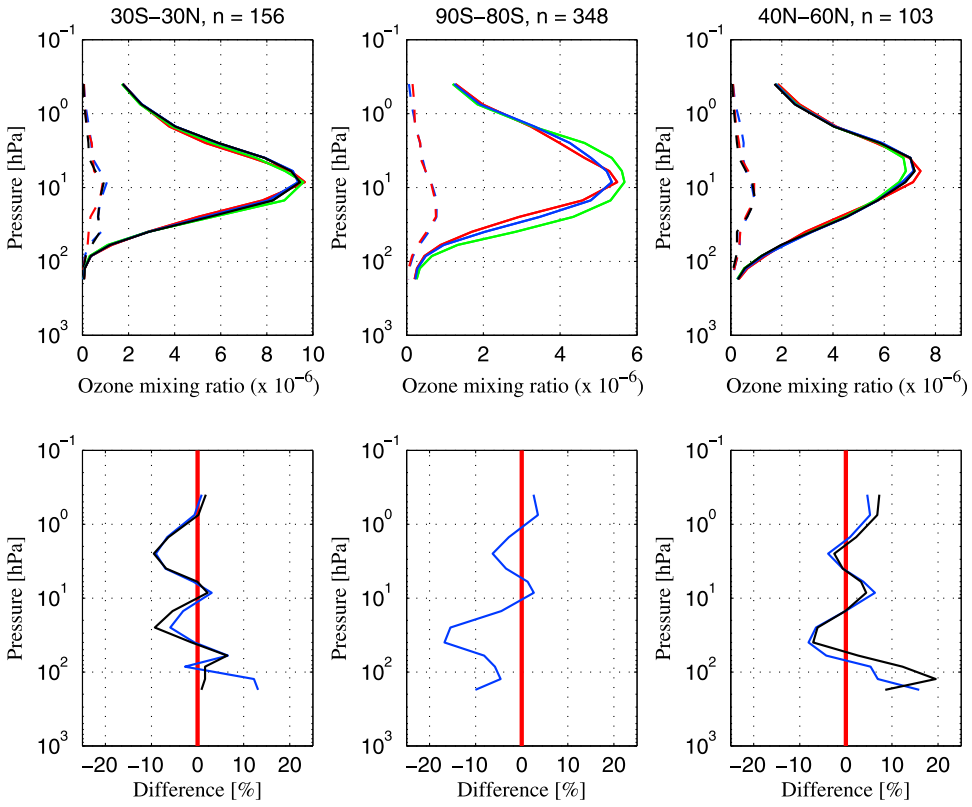


**Figure 17.** The results of satellite-satellite ozone profile comparisons. (top) Median ozone profiles (solid lines) of OMI (red), GOMOS (black), OSIRIS (blue) and OMI a-priori (green) accompanied by their standard deviations (dashed lines) for (right) October 2004, (middle) November 2006, and (left) September 2006. (bottom) Corresponding relative differences of GOMOS (black) and OSIRIS (blue) against OMI.

ozonesondes the SAGE-II data tends to show a slightly positive bias (~5%) between 15 km and 20 km altitude, and an increasing negative bias below the tropopause. The maximum negative bias reaches to ~30% at 8 km altitude. Although the SAGE-II (V6.1) ozone showed a large negative bias in the troposphere, *Kar et al.* [2002] showed that the SAGE-II ozone partial columns between 8 km and 17 km in the tropics have seasonal variations similar to those estimated from the NASA TOMS total ozone column data record [*Ziemke et al.*, 2001]. After adjusting estimated biases, the SAGE-II ozone data showed longitudinal wave-one structures in tropical troposphere [*Wang et al.*, 2002] similar to those observed from the ozonesonde data [*Thompson et al.*, 2003a]. This finding indicates that the low bias in SAGE-II tropospheric ozone above 8 km altitude is systematic and it could still provide useful climatological information after correcting for this systematic error. The major change in SAGE-II version 6.2 retrievals is to improve water vapor [*Thomason et al.*, 2004] where the impact on ozone is very small. Thus, all previously reported findings for SAGE-II version 6.1 ozone can also be applied to the version 6.2 data set employed here.

[20] *Bhatt et al.* [1999] validated HALOE version 18 vertical ozone profiles in the lower stratosphere with correlative ECC ozonesonde data. After filtering out potential aerosol/cirrus interference on HALOE ozone profiles and averaging/binning individual ozone profiles into 2.5 km layers, *Bhatt et al.* [1999] showed that HALOE version 18 ozone profiles agree well with coincident ozonesondes to within 10% over its entire vertical range from the upper stratosphere down to ~100 hPa. Unfortunately there has not been published a validation paper specifically for HALOE version 19 ozone profiles, but several studies indicate a low bias of HALOE version 19 in the lower stratosphere and troposphere. For example *Morris et al.* [2002] compared HALOE version 19 with SAGE-II V6.0 ozone by means of a trajectory mapping technique and found > 15% differences between the two data sets - with HALOE lower than SAGE-II - in the tropics below 22 km. HALOE version 19 ozone and SAOZ balloon profiles as launched in the tropics from the southern hemisphere stations show a very good agreement (within 1–2%) between 22 and 26 km [*Borchi et al.*, 2005; *Borchi and Pommereau*, 2007]. The agreement, however, degraded rapidly below 22 km where the difference increases up to ~40% at 18 km (in the tropics, with HALOE values being too low). This is consistent with comparisons between SAGE-II/HALOE and ozonesondes from *Wang et al.* [2006], where HALOE version 19 ozone shows much larger low biases than SAGE-II version 6.2 in the lower stratosphere and troposphere. In midlatitudes, the HALOE ozone starts showing negative biases below 17 to 18 km, and the bias increases to negative biases of ~10% and 20% at 15 km and 10 km, respectively. In the tropics, the HALOE ozone shows low bias of ~10% at 20 km and increases to approximately 50% at 15 km.

[21] The OMI retrieved ozone profiles are reported by subcolumn ozone [DU] in 18 pressure layers bounded between

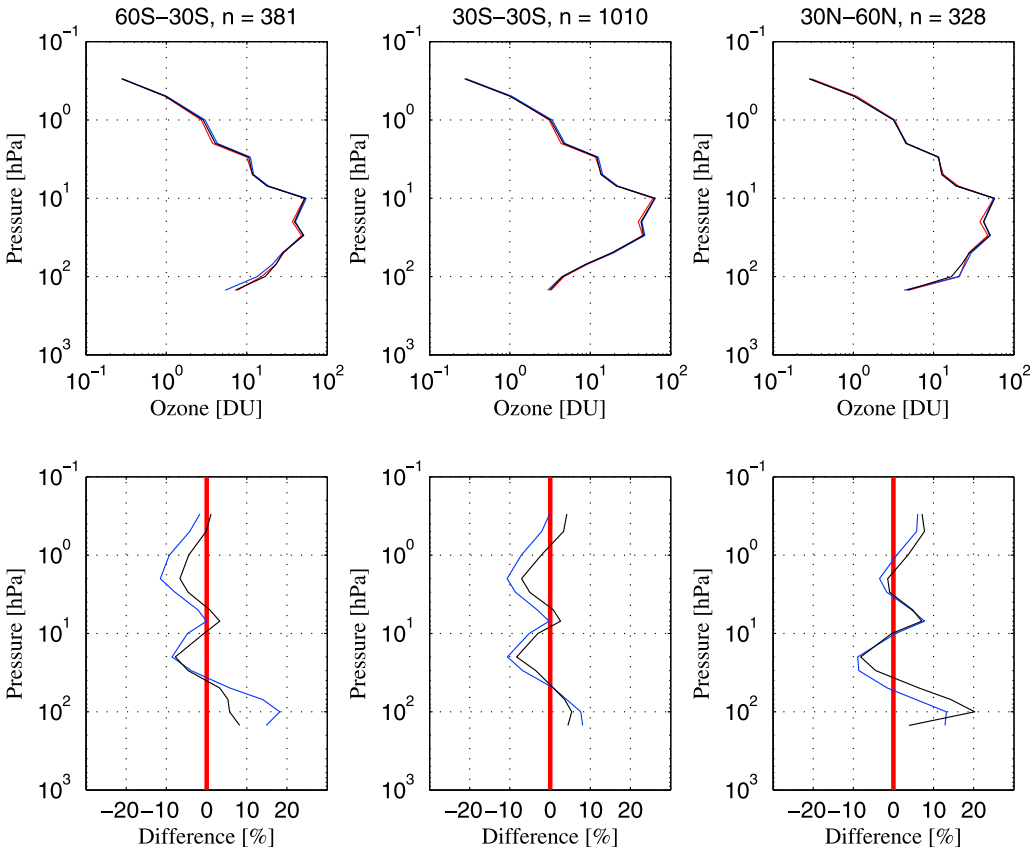


**Figure 18.** (top) The median ozone profiles in Dobson units for the entire year 2006 and (bottom) the corresponding relative differences. Colors are same as in Figure 17.

the Earth's surface elevation and 0.3 hPa. From the SAGE-II observations, however, one retrieves ozone number densities at geometric altitudes (i.e., expressed in km's) with a much higher vertical resolution of ~1 km. In order to compare SAGE-II and OMI, the SAGE-II ozone profiles were first converted to mixing ratios at pressure levels based on accompanied temperature and pressure profiles, which were derived from NCEP temperature/pressure data being interpolated to SAGE-II reported locations/times. The 18-layer ozone column version (in DU) of SAGE-II data can then be calculated following the method described before (see section 8). A similar approach was used here to convert the HALOE ozone profiles available at a vertical resolution of ~2.5 km to the 18-layer sub-ozone column version as used by OMI. We used collocation criteria of ±0.5 degree in both latitude and longitude and ±12 h in time to select coincident OMI and correlative SAGE-II/HALOE measurements. Both SAGE-II and HALOE ozone data were screened for possible aerosol/cloud contamination and other artifacts based on the recommendations and methods by *Wang et al.* [2002] and by *Bhatt et al.* [1999], respectively. Those OMI ozone profiles with the algorithm quality flag ProcessingQualityFlags set to values indicating problematic retrievals were also removed from our comparisons.

[22] The median differences and the statistical spreads between OMI and coincident SAGE-II ozone profiles are shown in Figure 14. The median and the statistical spread, defined as one half of differences between the 16th and 84th percentile differences, is the same as mean and standard deviation when the statistical sample has a Gaussian distribution [see, e.g., *Wang et al.*, 2002]. Medians and statistical spreads are less affected by anomalous differences in the lower stratosphere and upper troposphere which could result from noisy satellite measurements - due to the small ozone signal - and the strong natural dynamic variability not being completely eliminated due to spatial and temporal differences in measurements. Medians and statistical spreads therefore are used here for comparisons between OMI and other satellites and for comparisons against ozonesondes in later sections.

[23] The OMI and SAGE-II ozone show agreements of within ±10% from 0.3 hPa down to approximately 70 hPa (~18 km) between 30° and 60° latitude in both Hemispheres as is shown in Figure 14. Below 70 hPa, the OMI data shows positive biases relative to SAGE-II, with difference of approximately 20% at 70–100 hPa (~16 km) layer and 40% at 200–300 hPa (~9 km) layer. In the tropics the differences between OMI and SAGE-II show similar vertical structure as that in midlatitudes, with agreements of 10% or better between 0.3 and 50 hPa. (~20 km). The median differences again increase toward the lower stratosphere and the upper troposphere. It reaches ~20% at 70 hPa and ~60% at 100 hPa. The OMI ozone data also agrees with HALOE by 10% or better between 1 and 70 hPa as is shown in Figure 15. The differences become larger above pressures of 100 hPa, where OMI ozone values are greater than HALOE by 10 to 15%.

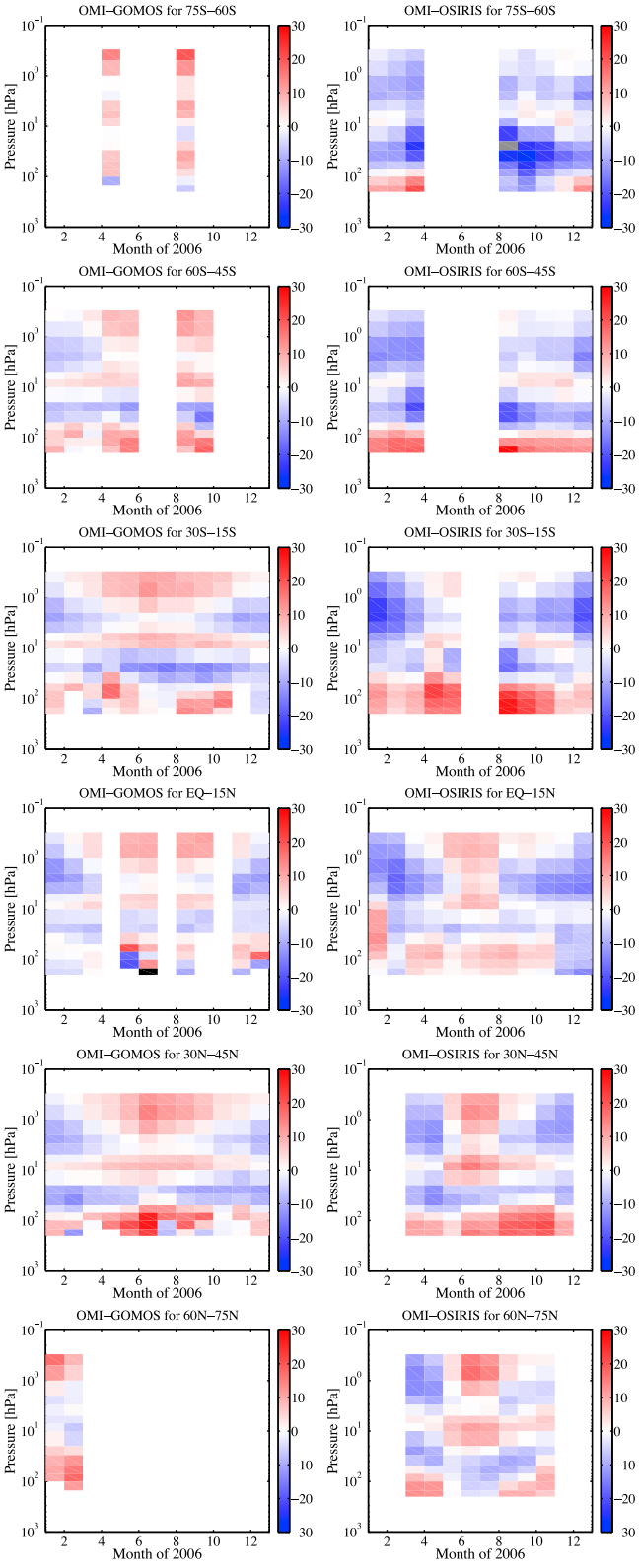


**Figure 19.** (left) OMI-GOMOS and (right) OMI-OSIRIS median relative differences calculated monthly for the entire year 2006 for selected latitude bins of 15° wide. Median number of profile pairs per month per latitude band is 418 for OMI-OSIRIS and 237 for OMI-GOMOS where month/latitude band combinations were not considered if less than 30 pairs were found.

These larger differences in upper stratospheric ozone mainly result from the low bias in HALOE, which had been shown in previous comparisons against SAGE-II/III [*Wang et al.*, 2006] and POAM III [*Randall et al.*, 2003]. Below 70 hPa in midlatitudes and 50 hPa in the tropics, OMI also shows positive biases (>30%) with respect to HALOE. Since both SAGE-II and HALOE have low biases relative to ozonesonde in the lower stratosphere and upper troposphere regions, we will compare OMI with ozonesonde directly in section 12 to evaluate its quality in that region.

## 11. Validation Against GOMOS and OSIRIS

[24] The Global Ozone Monitoring by the Occultation of Stars (GOMOS) is a limb viewing instrument on board the ESA-ENVISAT satellite [*Kyröla et al.*, 2004] that uses the stellar occultation technique to measure the vertical structure of the atmosphere. The main wavelength region of GOMOS is the ultraviolet-visible (UV-VIS) region 248–690 nm, which is used to retrieve vertical profiles of ozone and other trace gases. The vertical resolution of the GOMOS ozone profile is 2–3 km depending on altitude and the sampling resolution is 0.5–1.7 km. Nighttime measurements of GOMOS are in general of very good quality due to the absence of atmospherically scattered solar stray light. In the study of *Meijer et al.* [2004] GOMOS nighttime ozone profiles were compared to ground based microwave radiometer measurements, ECC balloon ozonesonde observations and ground based lidar measurements, where relatively small biases of 2,5% were found between 14 km and 45 km altitude, growing to a 7,5% between 45 km and 64 km altitude. In the recent study of *van Gijsel et al.* [2010] with the latest GOMOS data processing version 5.0, a very good agreement of ±2% was found against the before mentioned balloon ozonesonde measurements over the altitude range of 20 km to 40 km. The quality of an individual GOMOS profile logically depends on the type of star used in the occultation: In general the brightest stars yield the most accurate ozone profiles. In addition above 40 km the hot stars provide better results than the cool stars. A full description of the GOMOS algorithms is given by *Kyröla et al.* [2010] and a complete table of GOMOS data characteristics and error contributions is given by *Tamminen et al.* [2010].

[25] The Optical Spectrograph and Infrared Imager System (OSIRIS) is one of the two instruments on board the Swedish Odin satellite [*Llewellyn et al.*, 2004]. The spectrograph part of OSIRIS measures limb-scattered solar light in the UV-VIS-NIR wavelength region of 280–800 nm. At the Finnish Meteorological Institute (FMI) the vertical profiles of ozone, nitrogen dioxide (nitrite) and aerosols are processed from the OSIRIS measurements. The FMI-OSIRIS processing algorithm uses a Modified Onion Peeling inversion method [*Auvinen et al.*, 2002; *Tukiainen et al.*, 2008] with three peeling loops and uses the signal from 288 individual wavelength nodes. In the study of *Tukiainen et al.* [2008] a difference of 5% or less was found between OSIRIS day-time and GOMOS nighttime ozone profiles between 21 km and 45 km altitude. The vertical sampling resolution of OSIRIS is 1–3 km and the vertical resolution is 2–3 km depending on altitude. OSIRIS and GOMOS retrieval algorithms do not use a-priori ozone profile in the fitting routines; however, a-priori information is used otherwise: For OSIRIS a climatological

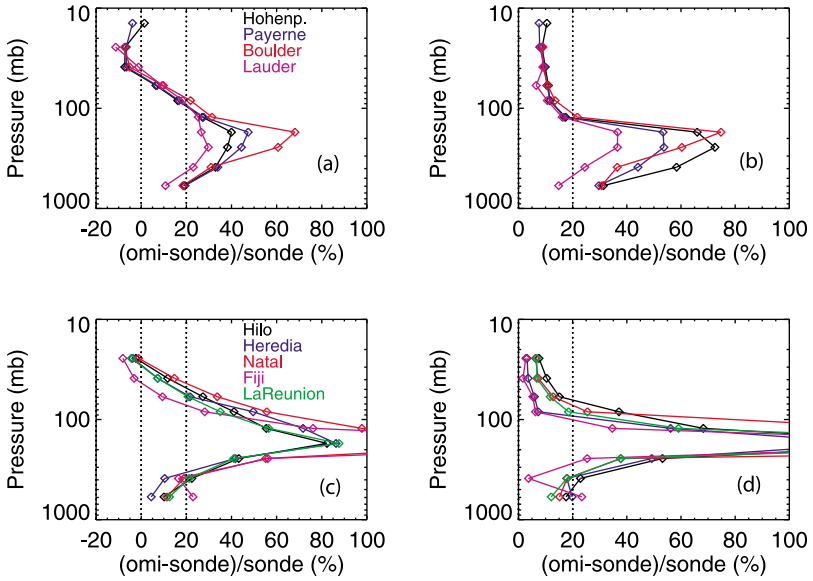


**Figure 20.** (a) Median relative differences and (b) statistical spreads between OMI and collocated ozonesondes at Hohenpeissenberg (black), Payerne (blue), Boulder (red) and Lauder (purple). (c, d) Similar comparison results between OMI and tropical ozonesondes at Hilo (black), Heredia (blue), Natal (red), Fiji (purple) and La Reunion (green).

atmosphere is assumed when creating the look-up tables for multiple scattering corrections. For GOMOS no explicit a-priori information is used, but the retrieved profile is assumed to be smooth and a technical smoothness prior is used by applying the Tikhonov regularization method in the vertical inversion [see, e.g., *Sofieva et al.*, 2004]. In this study we use the FMI-OSIRIS level-2 product version 2.1 and the GOMOS level-2 product version IPF 5.0. The OMI vertical ozone profiles are provided in Dobson units per layer in 18 different pressure layers. With GOMOS and OSIRIS the profiles are given in molecular number densities at a certain altitude. To compare GOMOS and OSIRIS ozone profiles with OMI ozone profiles we use the same methodology as with comparing OMI to MLS as explained in section 8. Hence GOMOS and OSIRIS vertical ozone profiles are weighted with the OMI averaging kernels but - vice versa - for OMI the weighting was not performed assuming that the vertical resolution of GOMOS and OSIRIS is sufficiently much higher to interpret their averaging kernels as delta functions. To transform GOMOS and OSIRIS ozone profiles from molecular number densities to volume mixing ratios we divide the ozone profiles by the ECMWF air density profiles that accompany the GOMOS and OSIRIS data products. ECMWF air density is provided every 6 h and interpolated to OSIRIS and GOMOS locations in the processing routines. The GOMOS product also comes with the ECMWF pressure levels. The pressure levels for OSIRIS are obtained by spline-interpolation of the OMI pressure levels, or copied from the ECMWF-GOMOS pressures, if available. In this study we only use GOMOS nighttime ozone profiles hence we should be careful when analyzing the results above 45 km where the diurnal variation of ozone becomes significant. As mentioned before, the quality of individual GOMOS measurements depends on the type of star used. Thus, we have selected only those occultations originating from stars brighter than magnitude 1.9 even though statistical studies imply that the mean ozone profiles retrieved from dimmer stars are not biased [*Meijer et al.*, 2004]. For every OSIRIS ozone profile we select the closest OMI ozone profile from the same day within a spatial difference of less than 1 degree in both latitude and longitude. To the same OSIRIS profile we find the closest GOMOS ozone profile that has a temporal difference less than 24 h and a longitudinal x latitudinal difference less than 5° × 2°, respectively. As an example we show in Figure 16 two 3-way ozone profile matches between OMI, GOMOS and OSIRIS.

[26] To measure the difference against OMI we define the relative difference as 100%*(OMI-{GOMOS,OSIRIS})/{GOMOS,OSIRIS}. In Figure 17 (left), the statistical analysis for October 2004 is shown. Between latitudes 30°N and 30°S some 156 3-way matches were found. The solid lines in the graphs represent the median profiles of each instrument and OMI a-priori. The corresponding standard deviations are shown in dashed lines. Please note the very similar differences of OSIRIS and GOMOS against OMI. We find minimal differences near the ozone peak and the difference maximizes around 2 hPa. Please note that over the entire vertical range the difference remains within ±10%. To study the southern

**Table 1.** Ground Based Ozonesonde Stations for Which the ECC Ozonesonde Ozone Profile Data Were Used to Compare With the OMI Satellite Based Ozone Profile Data

| Stations | Latitude | Longitude | Collocated Profiles |
|---|---|---|---|
| Hohenpeissenberg | 47.8° N | 11.02° E | 470 |
| Payerne | 46.49° N | 6.57° E | 454 |
| Boulder | 40.0° N | 254.75°E | 215 |
| Hilo | 19.4° N | 205.5° E | 148 |
| Heredia | 10.0° N | 275.89° E | 118 |
| Natal | 5.42° S | 324.6° E | 131 |
| Fiji | 18.13° S | 178.40° E | 60 |
| La Reunion | 21.06° S | 55.48° E | 89 |
| Lauder | 45.04° S | 169.68° E | 350 |

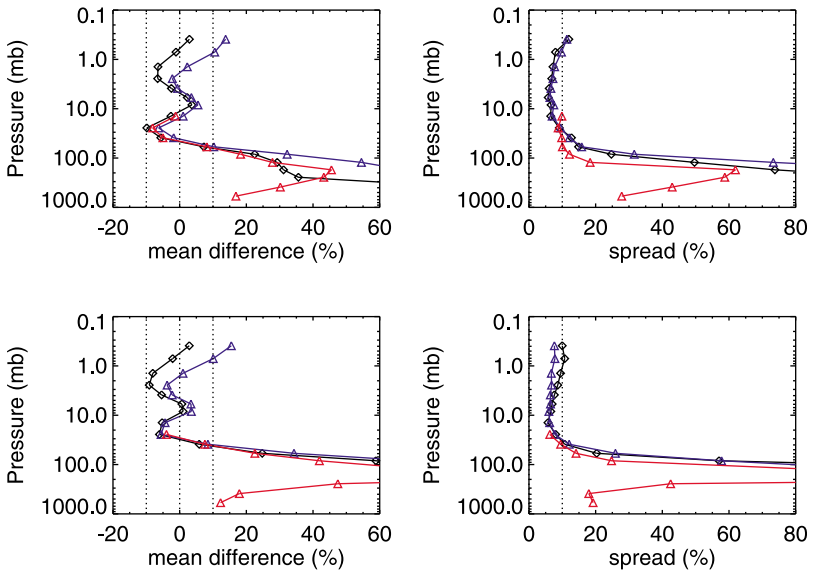


**Figure 21.** An overview of (left) mean relative differences and (right) statistical spreads between OMI and correlative SAGE-II (black), HALOE (blue), and ECC ozonesondes (red) in (top) midlatitudes and (bottom) the tropics.

polar region between the latitudes 80°S and 90°S we have selected the month of November 2006 which is part of a double record breaking ozone hole season. Unfortunately in this month and region no suitable GOMOS measurements were found and only OSIRIS measurements were used in the comparison. We found an appreciable 348 collocations and the statistical analysis is shown in the middle panel of Figure 17 where we plot the median OSIRIS and OMI profiles, their differences and their standard deviations. Below the ozone peak OMI sees roughly 15–20% less ozone than OSIRIS does while both data sets differ significantly from the OMI a-priori median profile. Last, we show the results from September 2006 in the latitude band between 40°N and 60°N where 103 3-way collocations were found. Again GOMOS and OSIRIS show very similar and systematic differences against OMI well within the ±10% range.

[27] In Figure 18 we show the overview for the entire year 2006 for the latitude bands 60°S-30°S, 30°S-30°N and 30°N-60°N where we found 381, 1010 and 328 3-way matches respectively. Again we note that, OSIRIS and GOMOS differences are well within the ±10% range above 100 hPa. We also note that, even though the differences have similar patterns in this longer analysis, in some places the OSIRIS-OMI difference is about 5% lower than the GOMOS-OMI difference. In Figure 19 we show monthly OMI-GOMOS and OMI-OSIRIS medians of differences for 2006 shown in the same way as for the weekly OMI-MLS differences in Figure 9. In this analysis we found the collocations separately and used same criteria for both instruments. We screened GOMOS only for the weakest segment and rejected the occultation if the star temperature was lower than 7000 K and at the same time the star magnitude was higher than 1.9. We considered the month and the latitude band only if 30 or more collocations were found. One should note that, even if the nominal latitude bands are 15 degrees, GOMOS measurements might be concentrated on very narrow latitude bands, depending on star used in the occultation. Also the number of found matches can be very different. Thus, a direct comparison between OMI-GOMOS, OMI-OSIRIS and OMI-MLS plots is difficult. One can note very similar structures in the differences especially with OMI-OSIRIS and OMI-MLS comparisons, indicating that the persistent structures are real and most likely OMI related. In many cases the monthly medians are within the ±10% range and in overall within ±20% except for the ozone hole conditions, whereas the OMI-OSIRIS difference can be over −30%. The median difference profiles show much variability at high latitudes and in the tropics and are relatively stable over middle latitudes on both hemispheres.

## 12. Validation Against ECC Ozonesondes

[28] The OMI V3.0 vertical ozone profiles were compared with ECC ozonesonde data from the World Ozone and Ultraviolet Radiation Data Centre (WOUDC) database, the Climate Monitoring & Diagnostics Laboratory (CMDL) and the Southern Hemisphere Additional Ozonesondes (SHADOZ) network. The actual ozonesonde data used in this study are listed in Table 1. Before comparing to the OMI vertical profiles, all ozonesonde data were integrated to ozone columns per layer based on the pressure levels as prescribed by OMI. In order to account for different vertical resolution, the OMI averaging kernels and a-priori information were applied to ozonesonde profiles [*Nassar et al.*, 2008; *Rodgers and Connor*, 2003]. The same coincident collocation criteria (±0.5° in latitude, ±0.5° in longitude, and ±12 h in time) as those in our satellite comparisons were used to choose collocated OMI and ozonesonde profiles. Median differences and statistical spreads between OMI and ozonesondes are shown in Figure 20 following the definitions introduced previously. Compared to three midlatitude ozonesonde stations in the northern hemisphere (Hohenpeissengerg, Payerne, Boulder), and one midlatitude ozonesonde station in the southern hemisphere (Lauder), OMI shows low biases of

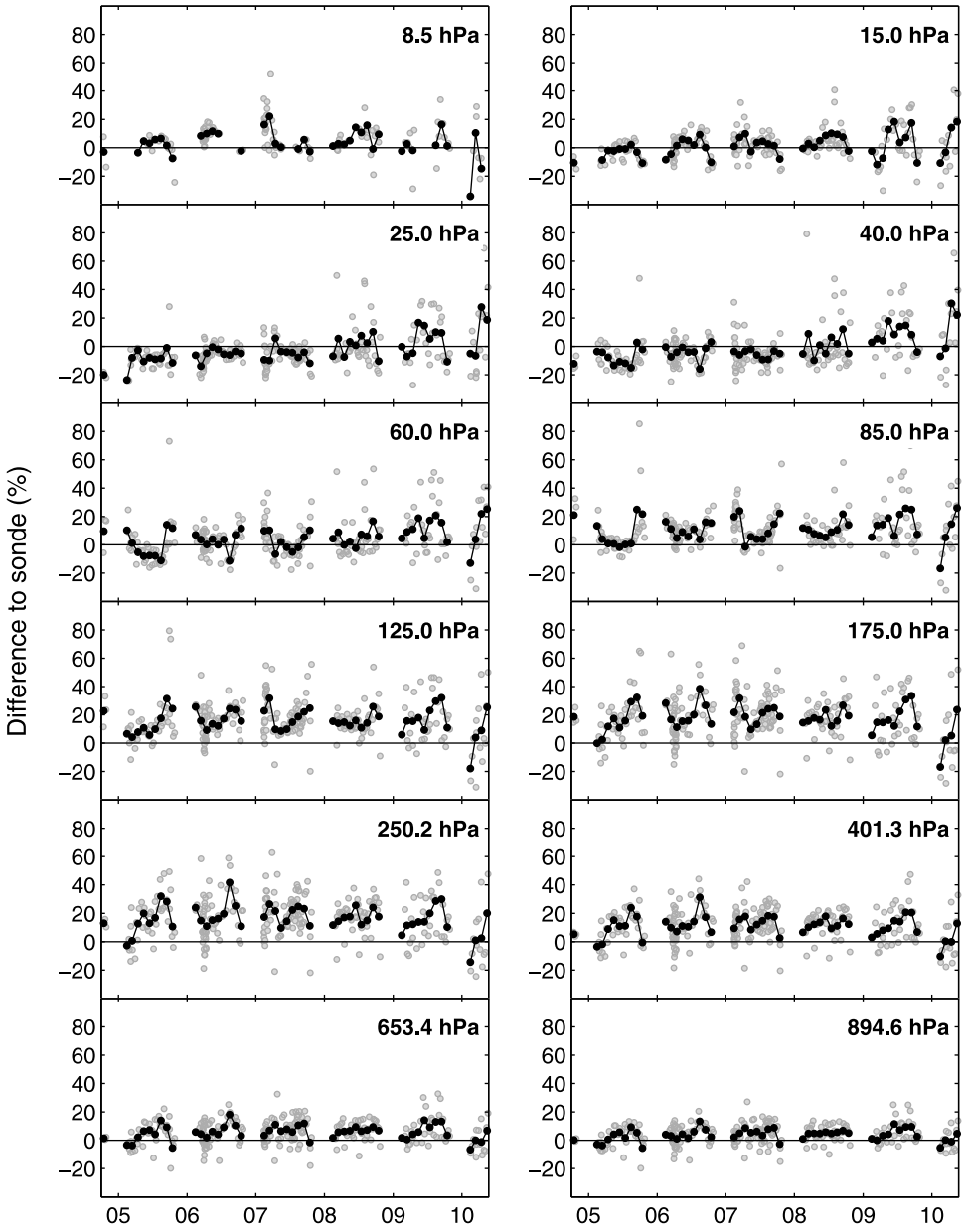


**Figure 22.** Time series of the OMI versus Sodankylä-sonde relative differences at OMI pressure layers from October 2004 to May 2010. The OMI averaging kernel and a-priori constraint has been applied to the ozone measured by the co-located ozonesonde data. Grey dots represent the collocated measurements and black dots correspond to the monthly averages of relative differences.

~5to 10% between 20 and 50 hPa as shown in Figure 20a. Below 50 hPa the OMI ozone values are generally larger than those reported by the ozonesonde, with the largest high bias of 50–60% in the 200–300 hPa layer. The spreads in OMI/sonde differences are mainly related to uncertainties in OMI measurements since ozonesonde uncertainties are typically estimated to be smaller than ~5%. Based on Figure 20b we estimate that OMI retrieved ozone profiles have precisions of ~5 to 10% between 10 and 50 hPa. Larger spreads below these levels could result from degraded precisions in OMI measurements and increasing dynamic variability. The effect of different dynamic variability on OMI/sonde comparisons can be seen clearly in the lower stratosphere and upper troposphere regions (e.g., between 100 and 300 hPa), where the variability of OMI/sonde differences in the southern hemisphere midlatitudes is much smaller than that in northern hemisphere midlatitudes (e.g., 40% versus 80% in 200 to 300 hPa layer)

[29] Comparisons between OMI and SHADOZ ozonesondes [*Thompson et al.*, 2003b] in the tropics showed similar vertical structures as those in the midlatitudes. Above 30 hPa OMI show negative bias of ~5 to 10% relative to ozonesonde (Figure 20c). Between 30 and 200 hPa altitude, OMI showed increasing positive biases, with the largest mean differences (~80% or more) at 125 to 175 hPa layer. The agreement between OMI and ozonesondes, however, became better

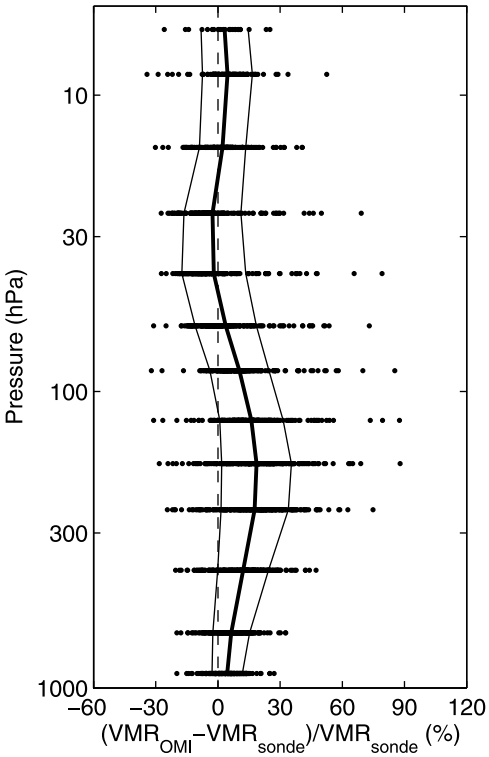


**Figure 23.** The average OMI-ECC ozonesonde profile relative differences for the Sodankylä ozonesonde data set covering the time frame October 1, 2004 to May 23, 2010. Ozonesonde data has been gridded on the OMI pressure level grid using the OMI averaging kernels. Black dots denote individual data points of all profiles, thick and thin black lines denote average and 1-sigma statistics, respectively.

below 200 hPa. The spreads of OMI/sonde differences in the tropics show similar vertical structures as mean differences, with the largest standard deviation (spread) between 100 and 200 hPa layer.

[30] An overview of averaged median differences and statistical spreads between OMI and SAGE-II, HALOE and ozonesondes are shown in Figure 21. The agreement between OMI and correlative measurements is shown to be within 10% down to 70 hPa in midlatitudes and 30 hPa in the tropics. In the lower stratosphere and in the troposphere, OMI ozone values are systematically larger than ozonesondes, with positive bias of ~20% and larger. The precisions (random error) of OMI retrieved ozone profiles are estimated to be 5–10% for altitudes above 30 hPa. The precision becomes worse below 30 hPa, and are approximately a factor of 4 to 6 worse between 100 and 200 hPa levels. The larger biases and worse precisions in the upper troposphere mainly result from OMI not having much vertical information in those regions, as can be seen by the lower values of the averaging kernels (i.e., Figure 1).

[31] It is of the highest importance to have accurate ozone observations over the polar regions as the effect of the Montreal protocol intended to reduce the atmospheric abundances of ozone depleting substances will manifest itself there most strongly. Our final validation exercise therefore consists of comparing OMI ozone profiles with the data from a single high-latitude station Sodankylä, Finland, located at (67.36° N, 26.63° E) that has in impressive data track record. The average difference of OMI ozone profiles to ECC ozonesonde data are shown in Figure 22 for a relatively long time period, from October 2004 to May 2010, where the OMI data has been thoroughly screened for the effects of the row anomaly and altogether 368 ozone soundings have been used. The variability can largely be explained by the natural variability of high-latitude ozone. The instrument precision of the ECC ozonesonde is better than 5% in the stratosphere and in Sodankylä the ozonesonde preparation procedure has not changed since the year 2004 [*Kivi et al.*, 2007]. Thus the ozonesonde time series could be used as reference time series to search for the possible trends and discontinuities in OMI data relative to the differences to ozonesonde over longer time period. From our OMI to ozonesonde comparisons, we do not find significant long-term trends in the differences. By taking the average of all collocated measurements we find a positive bias of OMI to the ozonesonde of less than 20% (at one sigma level) from 400 hPa down to 125 hPa. Below 400 hPa and above 85 hPa the bias was actually less than 10%. The average differences of OMI to the Sodankylä ozonesonde is shown in Figure 23.

## 13. Conclusions

[32] This paper has shown quantitatively that the quality of the OMI operational ozone profiles is sufficient for scientific explorations. The cross track averages per month of data show the OMI vertical ozone profiles to have persistent quality until at least December 2008 given the appropriate filtering for the ProcessingQualityFlags and XTrackQualityFlags fields. After mid-2009 the row anomaly seems to be affecting all cross track positions when above orbit phase 210° and we recommend not to use operational vertical ozone profile data above orbit phase 210° after June 2009.

[33] Co-flying OMI, MLS and TES - three very different types of remote sensing instruments with synergistic data products - aboard the Aura platform has proven to be extremely valuable for cross-validation. Validation against MLS shows that OMI is in agreement with MLS within ±10% for most latitudes except for the Polar regions during the ozone hole seasons where differences up to ±30% may occur. The persistent structures observed from the OMI-MLS difference plots and its absence in the validation plots of MLS versus SAGE-II, HALOE and ECC ozonesondes as published in the literature [*Froidevaux et al.*, 2006, 2008] leads us to believe that they originate solely from the OMI data. The persistent structures observed from the OMI-TES difference plots share the tropospheric and mesospheric features with the OMI-MLS comparison leading to the same conclusions. However, in the stratosphere OMI data has a slightly stronger negative bias against TES while showing some more structure against MLS. The validation of TES against ozonesondes as published by *Nassar et al.* [2008] shows a persistent positive bias of TES to the ozonesonde data that may explain our observations. TES has a positive bias in the UT of up to 15%, but otherwise agrees with the ozonesondes predicted by the error [*Boxe et al.*, 2010]. They find that for V003 and V004 versions TES ozone profiles are usually positively biased (less than 15%) in the troposphere and lower stratosphere and negatively biased in the middle stratosphere (less than 20%) when compared to ozonesonde data. However, in

most of the troposphere TES achieves excellent agreement against ozonesondes, leading to the same conclusions as OMI compared against MLS and ECC ozonesondes, namely that OMI overestimates tropospheric ozone abundances from 0 to 30%. Based on our experience with comparing OMI and TES ozone profile data it is our opinion that correcting for the difference in a-priori ozone profiles of the optimal estimation retrievals of two different satellite data sets with comparable vertical resolution of their averaging kernels following *Zhang et al.* [2010] is essential is achieving accurate and reliable results.

[34] Validation against SAGE-II and HALOE confirms the above statements and shows that OMI stratospheric ozone profiles are in agreement within ±10% for most latitudes. SAGE-II and HALOE are known to underestimate tropospheric ozone abundances hence partially explaining the larger deviations with OMI there. Validation against GOMOS and OSIRIS also shows that OMI stratospheric ozone profiles are in agreement within ±10% for most latitudes and confirms the origin of the persistent structures with altitude in the difference plots with OMI. Finally, the comparison against the ozonesonde data does show that in the troposphere OMI overestimates the ozone amounts often by more than 50%.

[35] Possible explanations for the above mentioned observations could be found in the corrections that are performed on the satellite level-1B reflectance data prior to the optimal estimation retrieval of the ozone profile, for example the correction for rotational Raman scattering - or Cabannes scattering. When applied too vigorously the correction might remove too much light from the spectrum such that the algorithm will overestimate ozone to account for this, particularly in the troposphere. The same reasoning holds for the stray light correction which performs a correction for the scattering of light of other wavelengths onto the detector in the UV1 wavelength range by the imperfect OMI optics; the accuracy of this correction is of crucial importance at these very low signal levels. And finally one my ask whether we dealing with clouds correctly by estimating their albedo from the Level-1B data and importing their effective cloud top pressure from the OMI $O_2$-$O_2$ cloud retrieval that is performed at the longest wavelengths in the OMI visible channel, i.e., at the other end of the OMI electromagnetic spectrum.

[36] We consider a comparison with the OMI scientific ozone profile data product as retrieved by *Liu et al.* [2010a] to be beyond the scope of this work at present. Although the OMI operational ozone profile retrieval is based on the same principles of optimal estimation we do not adjust the OMI level-1B reflectance prior to the retrieval by soft-calibration methods based on modeling of the Earth's reflectance where MLS ozone profiles are ingested. In our view the OMI scientific ozone profiles are a stand alone data product not suitable for the validation purposes of this paper as the focus would shift to algorithmic approach differences rather than this assessment of the quality of the OMI operational ozone profiles.

[37] **Acknowledgments.** The Dutch-Finnish built Ozone Monitoring Instrument (OMI) is part of the National Aeronautics and Space Administration (NASA) Earth Observing System (EOS) Aura satellite payload. The OMI project is managed by the Netherlands Space Office (NSO) and the Royal Netherlands Meteorological Institute (KNMI). OMI vertical ozone profile data were processed at and obtained from the NASA Goddard Earth Sciences (GES) Data and Information Services Center (DISC). The work of M. Kroon, J.P. Veefkind and J.F de Haan was supported by the Netherlands Space Organization via the EOS-Aura OMI Science project. The work by L. Froidevaux and the MLS team at the Jet Propulsion Laboratory, California Institute of Technology, was performed under contract with the National Aeronautics and Space Administration. The work of R. Wang was supported by Georgia Institute of Technology (Georgia-Tech) via the EOS-Aura OMI Science project. The work of J. Hakkarainen has been supported by the Academy of Finland's NOVAC project. The work of R. Kivi has been supported by the Finnish Meteorological Institute (FMI) via the EOS-Aura OMI Science project. We thank Susan S. Kulawick of the TES team for stimulating discussions. We wish to thank Lin Zhang of Harvard University for providing us with the code for correcting our OMI-TES comparisons for the a-priori differences. We wish to thank the three anonymous reviewers whose input made this paper stronger and more useful. We dedicate this work to the memory of Derek Martin Cunnold, who devoted his scientific career to the understanding of the dynamics and chemistry of atmospheric ozone.

## References

Auvinen, H., L. Oikarinen, and E. Kyrölä (2002), Inversion algorithms for recovering minor species densities from limb scatter measurements at UV-visible wavelengths, *J. Geophys. Res.*, *107*(D13), 4172, doi:10.1029/2001JD000407.

Bhartia, P. K., R. D. McPeters, C. L. Mateer, L. E. Flynn, and C. Wellemeyer (1996), Algorithm for the estimation of vertical ozone profiles from the backscattered ultraviolet technique, *J. Geophys. Res.*, *101*(D13), 18,793–18,806, doi:10.1029/96JD01165.

Bhatt, P. P., E. E. Remsberg, L. L. Gordley, J. M. McInerney, V. G. Brackett, and J. M. Russell III (1999), An evaluation of the quality of Halogen Occultation Experiment ozone profiles in the lower stratosphere, *J. Geophys. Res.*, *104*(D8), 9261–9275, doi:10.1029/1999JD900058.

Borchi, F., and J.-P. Pommereau (2007), Evaluation of ozonesondes, HALOE, SAGE-II and III, Odin-OSIRIS and -SMR, and ENVISAT-GOMOS, -SCIAMACHY and -MIPAS ozone profiles in the tropics from SAOZ long duration balloon measurements in 2003 and 2004, *Atmos. Chem. Phys.*, *7*, 2671–2690, doi:10.5194/acp-7-2671-2007.

Borchi, F., J. P. Pommereau, A. Gamier, and M. Nunes-Pinhanrada (2005), Evaluation of SHADOZ ozonesondes, HALOE and SAGE-II ozone profiles at the tropics from SAOZ UV-Vis remote measurements onboard long duration balloons, *Atmos. Chem. Phys.*, *5*, 1381–1397, doi:10.5194/acp-5-1381-2005.

Boxe, C. S., et al. (2010), Validation of northern latitude Tropospheric Emission Spectrometer stare ozone profiles with ARC-IONS ozonesondes during ARCTAS: Sensitivity, bias and error analysis, *Atmos. Chem. Phys.*, *10*, 9901–9914, doi:10.5194/acp-10-9901-2010.

Chance, K. V., J. P. Burrows, D. Perner, and W. Schneider (1997), Satellite measurements of atmospheric ozone profiles, including tropospheric ozone, from ultraviolet/visible measurements in the nadir geometry: A potential method to retrieve tropospheric ozone, *J. Quant. Spectrosc. Radiat. Transfer*, *57*(4), 467–476, doi:10.1016/S0022-4073(96)00157-4.

Cunnold, D. M., W. P. Chu, R. A. Barnes, M. P. McCormick, and R. E. Veiga (1989), Validation of SAGE II ozone measurements, *J. Geophys. Res.*, *94*(D6), 8447–8460, doi:10.1029/JD094iD06p08447.

de Haan, J. F., P. B. Bosma, and J. W. Hovenier (1987), The adding method for multiple scattering calculations of polarized light, *Astron. Astrophys.*, *183*, 371–391.

Dirksen, R., M. R. Dobber, R. Voors, and P. F. Levelt (2006), Prelaunch characterization of the Ozone Monitoring Instrument transfer function in the spectral domain, *Appl. Opt.*, *45*, 3972–3981, doi:10.1364/AO.45.003972.

Dobber, M., R. Voors, R. Dirksen, Q. Kleipool, and P. Levelt (2008), The high-resolution solar reference spectrum between 250 and 550 nm and its application to measurements with the Ozone Monitoring Instrument, *Sol. Phys.*, *249*, 281–291, doi:10.1007/s11207-008-9187-7.

Froidevaux, L., et al. (2006), Early validation analyses of atmospheric profiles from EOS MLS on the Aura satellite, *IEEE Trans. Geosci. Remote Sens.*, *44*(5), 1106–1121, doi:10.1109/TGRS.2006.864366.

Froidevaux, L., et al. (2008), Validation of Aura Microwave Limb Sounder stratospheric ozone measurements, *J. Geophys. Res.*, *113*, D15S20, doi:10.1029/2007JD008771.

Hasekamp, O. P., and J. Landgraf (2001), Ozone profile retrieval from backscattered ultraviolet radiances: The inverse problem solved by regularization, *J. Geophys. Res.*, *106*(D8), 8077–8088, doi:10.1029/2000JD900692.

Hoogen, R., V. V. Rozanov, and J. P. Burrows (1999), Ozone profiles from GOME satellite data: Algorithm description and first validation, *J. Geophys. Res.*, *104*(D7), 8263–8280, doi:10.1029/1998JD100093.

Jiang, Y. B., et al. (2007), Validation of Aura Microwave Limb Sounder ozone by ozonesonde and lidar measurements, *J. Geophys. Res.*, *112*, D24S34, doi:10.1029/2007JD008776.

Kar, J., C. R. Trepte, L. W. Thomason, J. M. Zawodny, D. M. Cunnold, and H. J. Wang (2002), On the tropospheric measurements by the Stratospheric Aerosol and Gas Experiment II (SAGE-II, version 6.1) in the tropics, *Geophys. Res. Lett.*, *29*(24), 2208, doi:10.1029/2002GL016241.

Kivi, R., E. Kyrö, T. Turunen, N. R. P. Harris, P. von der Gathen, M. Rex, S. B. Andersen, and I. Wohltmann (2007), Ozonesonde observations in the Arctic during 1989–2003: Ozone variability and trends in the lower stratosphere and free troposphere, *J. Geophys. Res.*, *112*, D08306, doi:10.1029/2006JD007271.

Kleipool, Q. L., M. R. Dobber, J. F. de Haan, and P. F. Levelt (2008), Earth surface reflectance climatology from 3 years of OMI data, *J. Geophys. Res.*, *113*, D18308, doi:10.1029/2008JD010290.

Kroon, M., J. P. Veefkind, M. Sneep, R. D. McPeters, P. K. Bhartia, and P. F. Levelt (2008), Comparing OMI-TOMS and OMI-DOAS total ozone column data, *J. Geophys. Res.*, *113*, D16S28, doi:10.1029/2007JD008798.

Kyrölä, E., et al. (2004), GOMOS on Envisat: An overview, Adv. *Space Res.*, *33*(7), 1020–1028, doi:10.1016/S0273-1177(03)00590-8.

Kyrölä, E., et al. (2010), Retrieval of atmospheric parameters from GOMOS data, *Atmos. Chem. Phys. Discuss.*, *10*, 10,145–10,217, doi:10.5194/acpd-10-10145-2010.

Levelt, P. F., G. H. J. van den Oord, M. R. Dobber, A. Malkki, H. Visser, J. de Vries, P. Stammes, J. O. V. Lundell, and H. Saari (2006a), The Ozone Monitoring Instrument, *IEEE Trans. Geosci. Remote Sens.*, *44*(5), 1093–1101, doi:10.1109/TGRS.2006.872333.

Levelt, P. F., E. Hilsenrath, G. W. Leppelmeier, G. H. J. van den Oord, P. K. Bhartia, J. Tamminen, J. F. de Haan, and J. P. Veefkind (2006b), Science objectives of the Ozone Monitoring Instrument, *IEEE Trans. Geosci. Remote Sens.*, *44*(5), 1199–1208, doi:10.1109/TGRS.2006.872336.

Liu, X., K. Chance, C. E. Sioris, R. J. D. Spurr, T. P. Kurosu, and R. V. Martin (2005), Ozone profile and tropospheric ozone retrievals from the Global Ozone Monitoring Experiment: Algorithm description and validation, *J. Geophys. Res.*, *110*, D20307, doi:10.1029/2005JD006240.

Liu, X., P. K. Bhartia, K. Chance, R. J. D. Spurr, and T. P. Kurosu (2010a), Ozone profile retrievals from the Ozone Monitoring Instrument, *Atmos. Chem. Phys.*, *10*, 2521–2537, doi:10.5194/acp-10-2521-2010.

Liu, X., P. K. Bhartia, K. Chance, L. Froidevaux, R. J. D. Spurr, and T. P. Kurosu (2010b), Validation of Ozone Monitoring Instrument (OMI) ozone profiles and stratospheric ozone columns with Microwave Limb Sounder (MLS) measurements, *Atmos. Chem. Phys.*, *10*, 2539–2549, doi:10.5194/acp-10-2539-2010.

Livesey, N. J., et al. (2008), Validation of Aura Microwave Limb Sounder $O_3$ and CO observations in the upper troposphere and lower stratosphere, *J. Geophys. Res.*, *113*, D15S02, doi:10.1029/2007JD008805.

Llewellyn, E. J., et al. (2004), The OSIRIS instrument on the Odin spacecraft, *Can. J. Phys.*, *82*, 411–422, doi:10.1139/P04-005.

Malicet, C., D. Daumont, J. Charbonnier, C. Parisse, A. Chakir, and J. Brion (1995), Ozone UV spectroscopy, II. Absorption cross-sections and temperature dependence, *J. Atmos. Chem.*, *21*, 263–273, doi:10.1007/BF00696758.

McCormick, M. P., J. M. Zawodny, R. E. Veiga, J. C. Larsen, and P. H. Wang (1989), An overview of SAGE I and II ozone measurements, *Planet. Space Sci.*, *37*(12), 1567–1586, doi:10.1016/0032-0633(89)90146-3.

McPeters, R. D., G. J. Labow, and J. A. Logan (2007), Ozone climatological profiles for satellite retrieval algorithms, *J. Geophys. Res.*, *112*, D05308, doi:10.1029/2005JD006823.

Meijer, Y. J., et al. (2004), Pole-to-pole validation of Envisat GOMOS ozone profiles using data from ground-based and balloon ozonesonde measurements, *J. Geophys. Res.*, *109*, D23305, doi:10.1029/2004JD004834.

Mijling, B., O. N. E. Tuinder, R. F. van Oss, and R. J. van der A (2010), Improving ozone profile retrieval from spaceborne UV backscatter spectrometers using convergence behaviour diagnostics, *Atmos. Meas. Tech.*, *3*, 1555–1568, doi:10.5194/amt-3-1555-2010.

Morris, G. A., J. F. Gleason, J. M. Russell III, M. R. Schoeberl, and M. P. McCormick (2002), A comparison of HALOE version 19 with SAGE-II V6.00 ozone observations using trajectory mapping, *J. Geophys. Res.*, *107*(D13), 4177, doi:10.1029/2001JD000847.

Müller, M. D., A. K. Kaifel, M. Weber, S. Tellmann, J. P. Burrows, and D. Loyola (2003), Ozone profile retrieval from Global Ozone Monitoring Experiment (GOME) data using a neural network approach (Neural Network Ozone Retrieval System (NNORSY)), *J. Geophys. Res.*, *108*(D16), 4497, doi:10.1029/2002JD002784.

Munro, R., R. Siddans, W. J. Reburn, and B. Kerridge (1998), Direct measurement of tropospheric ozone from space, *Nature*, *392*, 168–171, doi:10.1038/32392.

Nassar, R., et al. (2008), Validation of Tropospheric Emission Spectrometer (TES) nadir ozone profiles using ozonesonde measurements, *J. Geophys. Res.*, *113*, D15S17, doi:10.1029/2007JD008819.

Osterman, D. (Ed.) (2009), Earth Observing System (EOS) Tropospheric Emission Spectrometer (TES) Level 2 (L2) data user's guide–Version 4, *Rep. D-38042*, 66 pp., NASA Jet Propul. Lab., Pasadena, Calif. [Available at http://tes.jpl.nasa.gov/uploadedfiles/TESDataUsersGuideV4_0.pdf.]

Randall, C. E., et al. (2003), Validation of POAM III ozone: Comparisons with ozonesonde and satellite data, *J. Geophys. Res.*, *108*(D2), 4367, doi:10.1029/2002JD002944.

Rodgers, C. D. (2000), *Inverse Methods for Atmospheric Sounding—Theory and Practice*, World Sci., Singapore.

Rodgers, C. D., and B. J. Connor (2003), Intercomparison of remote sounding instruments, *J. Geophys. Res.*, *108*(D3), 4116, doi:10.1029/2002JD002299.

Russell, J. M., III, L. L. Gordley, J. H. Park, S. R. Drayson, D. H. Hesketh, R. J. Cicerone, A. F. Tuck, J. E. Frederick, J. E. Harries, and P. Crutzen (1993), The Halogen Occultation Experiment, *J. Geophys. Res.*, *98*(D6), 10,777–10,797, doi:10.1029/93JD00799.

Schoeberl, M. R., et al. (2006), Overview of the EOS-Aura Mission, *IEEE Trans. Geosci. Remote Sens.*, *44*(5), 1066–1074, doi:10.1109/TGRS.2005.861950.

Sofieva, V. F., J. Tamminen, H. Haario, E. Kyrölä, and M. Lehtinen (2004), Ozone profile smoothness as a-priori information in the inversion of limb measurements, *Ann. Geophys.*, *22*, 3411–3420, doi:10.5194/angeo-22-3411-2004.

Tamminen, J., et al. (2010), GOMOS data characterization and error estimation, *Atmos. Chem. Phys. Discuss.*, *10*, 6755–6796, doi:10.5194/acpd-10-6755-2010.

Thomason, L. W., S. P. Burton, N. Iyer, J. M. Zawodny, and J. Anderson (2004), A revised water vapor product for the Stratospheric Aerosol and Gas Experiment (SAGE) II version 6.2 data set, *J. Geophys. Res.*, *109*, D06312, doi:10.1029/2003JD004465.

Thompson, A. M., et al. (2003a), Southern Hemisphere Additional Ozonesondes (SHADOZ) 1998–2000 tropical ozone climatology: 2. Tropospheric variability and the zonal wave-one, *J. Geophys. Res.*, *108*(D2), 8241, doi:10.1029/2002JD002241.

Thompson, A. M., et al. (2003b), The 1998–2000 southern Hemisphere Additional Ozonesondes (SHADOZ) tropical ozone climatology: 1. Comparison with TOMS and ground-based measurements, *J. Geophys. Res.*, *108*(D2), 8238, doi:10.1029/2001JD000967.

Tukiainen, S., S. Hassinen, A. Seppälä, H. Auvinen, E. Kyrölä, J. Tamminen, C. S. Haley, N. Lloyd, and P. T. Verronen (2008), Description and validation of a limb scatter retrieval method for Odin/OSIRIS, *J. Geophys. Res.*, *113*, D04308, doi:10.1029/2007JD008591.

van der A, R. J., R. F. van Oss, A. J. M. Piters, J. P. F. Fortuin, Y. J. Meijer, and H. M. Kelder (2002), Ozone profile retrieval from recalibrated GOME data, *J. Geophys. Res.*, *107*(D15), 4239, doi:10.1029/2001JD000696.

van Gijsel, J. A. E., et al. (2010), GOMOS ozone profile validation using ground-based and balloon ozonesonde measurements, *Atmos. Chem. Phys. Discuss.*, *10*, 8515–8551, doi:10.5194/acpd-10-8515-2010.

van Oss, R. F., and R. J. D. Spurr (2002), Fast and accurate 4 and 6 stream linearized discrete ordinate radiative transfer models for ozone profile retrieval, *J. Quant. Spectrosc. Radiat. Transfer*, *75*, 177–220, doi:10.1016/S0022-4073(01)00246-1.

van Oss, R. F., R. H. M. Voors, and R. J. D. Spurr (2001), Ozone profile algorithm, in *OMI Algorithm Theoretical Basis Document*, vol. 2, *OMI Ozone Products*, edited by P. K. Bhartia, pp. 51–73, NASA Goddard Space Flight Cent., Greenbelt, Md.

van Peet, J. C. A., R. J. van der A, A. T. J. de Laat, O. N. E. Tuinder, G. König-Langlo, and J. Wittig (2009), Height resolved ozone hole structure as observed by the Global Ozone Monitoring Experiment–2, *Geophys. Res. Lett.*, *36*, L11816, doi:10.1029/2009GL038603.

Wang, H. J., D. M. Cunnold, L. W. Thomason, J. M. Zawodny, and G. E. Bodeker (2002), Assessment of SAGE version 6.1 ozone data quality, *J. Geophys. Res.*, *107*(D23), 4691, doi:10.1029/2002JD002418.

Wang, H. J., D. M. Cunnold, C. Trepte, L. W. Thomason, and J. M. Zawodny (2006), SAGE-III solar ozone measurements: Initial results, *Geophys. Res. Lett.*, *33*, L03805, doi:10.1029/2005GL025099.

Waters, J. W., et al. (2006), The Earth Observing System Microwave Limb Sounder (EOS MLS) on the Aura satellite, *IEEE Trans. Geosci. Remote Sens.*, *44*(5), 1075–1092, doi:10.1109/TGRS.2006.873771.

Zhang, L., D. J. Jacob, X. Liu, J. A. Logan, K. Chance, A. Eldering, and B. R. Bojkov (2010), Intercomparison methods for satellite measurements of atmospheric composition: Application to tropospheric ozone

from TES and OMI, *Atmos. Chem. Phys.*, *10*, 4725–4739, doi:10.5194/acpd-10-1417-2010.

Ziemke, J. R., S. Chandra, and P. K. Bhartia (2001), "Cloud Slicing": A new technique to derive upper tropospheric ozone from satellite measurements, *J. Geophys. Res.*, *106*(D9), 9853–9867, doi:10.1029/2000JD900768.

J. F. de Haan, M. Kroon, and J. P. Veefkind, Department of Climate and Seismology, Royal Netherlands Meteorological Institute, PO Box 201, NL-3730 AE De Bilt, Netherlands. (mark.kroon@knmi.nl)

L. Froidevaux, Jet Propulsion Laboratory, California Institute of Technology, MS 183-701, 4800 Oak Grove Dr., Pasadena, CA 91109, USA.

J. J. Hakkarainen, Department of Earth Observation, Finnish Meteorological Institute, PO Box 503, FIN-00101 Helsinki, Finland.

R. Kivi, Arctic Research Centre, Finnish Meteorological Institute, Tähteläntie 62, FIN-99600, Sodankylä, Finland.

R. Wang, School of Earth and Atmospheric Sciences, Georgia Institute of Technology, Atlanta, GA 30332-0340, USA.